Finite Elements in Analysis and Design 227 (2023) 104041

Contents lists available at ScienceDirect

Finite Elements in Analysis & Design

journal homepage: www.elsevier.com/locate/finel

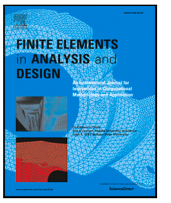

# Rigorous code verification for non-linear Kirchhoff–Love shells based on tangential differential calculus with application to Isogeometric Analysis

M.H. Gfrerer

*Institute of Applied Mechanics, Graz University of Technology, Technikerstrasse 4, 8010 Graz, Austria*

ARTICLE INFO

*Keywords:*
Shells
IGA
Surface balance laws
Verification
Tangential differential calculus
Manufactured solution

ABSTRACT

In order to ensure the reliability of a numerical simulation software, verification and validation are unavoidable tasks. In this paper, we present a new rigorous code verification strategy based on manufactured solutions for the static analysis of geometrically non-linear Kirchhoff–Love shells and apply it to Isogeometric Analysis (IGA). While IGA is based on a parametric surface description, we advocate to base the manufactured solutions on a parametrization-free formulation. To this end the governing equations in strong form are derived based on first principles of continuum mechanics using tangential differential calculus (TDC). This formulation bypasses the need of a parametrization. Therefore, the code verification and the IGA are decoupled, which makes the verification more rigorous. A second advantage of the circumvention of a parametrization are simpler and more stable to evaluate resulting forcing functions. The proposed code verification is performed for several examples and optimal convergence rates are obtained.

## 1. Introduction

Thin shells are key components in many engineering applications such as aircraft design, automotive industry, and architectural construction. We refer to [1–3] and references therein for an overview of different models of shells. In order to ensure the reliability of numerical results of computational models, rigorous verification and validation are unavoidable tasks [4,5]. Here, we focus on the task of code verification, which represents the process of demonstrating that the governing equations are solved consistently by the implemented method. Following the review in [6], the different criteria for assessing code verification are, in order of increasing rigor: expert judgment, error quantification, consistency/convergence, and order-of-accuracy. Thus, the order-of-accuracy test is the recommended acceptance test for rigorous code verification [5,7]. However, state-of-the-art verification tests in shell analysis, like the so-called "shell obstacle course" [8], suffer from lack of rigor. Typically, in these error quantification and convergence tests the displacement or stress fields are compared to reference values at particular spatial locations. As these reference values are also obtained by numerical methods, the accuracy is low. In order to perform order-of-accuracy tests, exact solutions for the governing equations are needed. To obtain such solutions, a technique called the *method of manufactured solutions* (first presented in [9]) can be used. Its central idea is to prescribe a solution and to determine an artificial source term, which is added to the governing equations, such that the modified equations are fulfilled for the prescribed solution. To the best of the author's knowledge, rigorous code verification based on manufactured solutions has only been performed for linear Kirchhoff–Love shells [10–12] but not for non-linear Kirchhoff–Love shells. Thus, in the present paper we extend the concept of manufactured solutions based on implicit geometry descriptions in [12] to non-linear Kirchhoff–Love shells.

*E-mail address:* gfrerer@tugraz.at.

https://doi.org/10.1016/j.finel.2023.104041
Received 19 May 2023; Received in revised form 4 September 2023; Accepted 5 September 2023
Available online 16 September 2023

Classically, the governing equations are given in local coordinates, *i.e.* it is assumed that a (global) parametrization of the shell surface is available and the equations are written component-wise, see e.g. [13] or [14]. While formulations based on parametrizations are natural for classical surface finite element methods and IGA, formulations circumventing a parametrization are interesting (i) from a theoretical point of view, (ii) for unfitted finite element methods [12,15–19], and (iii) the generation of manufactured solutions proposed in the present paper. We remark that for a given surface infinite many parametrizations are possible, and thus a formulation without a parametrization is of theoretical interest. Several coordinate-free formulations for different partial differential equations on surfaces (or more general manifolds) are available. Here, we focus on structural mechanics. In the early paper [20] a coordinate-free non-linear membrane theory is presented. Formulations based on TDC, where global coordinates are used, has been proposed for linear membranes [21], non-linear membranes [22], optimal design of membranes [23], linear Kirchhoff–Love shells [12,24] and non-linear Kirchhoff–Love shells [25]. However, in [25] only the weak formulation is reformulated in a parametrization-free way and no strong form is provided. Thus, one novelty of the present paper is the formulation of the governing equations of non-linear Kirchhoff–Love shells in strong form.

The Kirchhoff–Love shell model yields a vector-valued fourth-order partial differential equation. Therefore, for a conforming discretization of the fourth-order equation $C^1$ continuous shape functions are needed. However, for general unstructured meshes it is not possible to ensure $C^1$-continuity with only local polynomial shape functions and the nodal degrees of freedom consist of displacements and slopes only [26]. Therefore, different non-standard triangular elements developed for thin plate bending are the Argyris element [27,28], the Bell element [29] or the Clough–Tocher macro-triangle [30]. A further possibility to construct $C^1$-continuous approximation spaces on a general space triangulation relies on sophisticated techniques from subdivision surfaces [31]. However, on a structured quadrilateral mesh the Bogner–Fox–Schmit element [32,33] is a simple conforming element. The constraint of a structured quadrilateral mesh can be partially overcome by introducing a smooth mapping of the geometry [10]. This idea can be realized in an isoparametric way by the use of splines for the geometry mapping and for the discretization of the displacement field as it is done in IGA [34,35]. The general difficulty of constructing $C^1$-continuous approximation spaces led to approaches where the $C^1$-continuity requirement is circumvented. Among them we mention discrete Kirchhoff elements [36,37], where the Kirchhoff constraint is enforced only at discrete points, the use of shear-deformable (Reissner–Mindlin) shell theory [38,39], where only $C^0$-continuity approximation spaces are required, mixed methods [40,41], continuous/discontinuous Galerkin methods [42,43] and others. In the present paper we use the single-patch IGA formulation from [35] for the discretization of the Kirchhoff–Love shell problem. Thus, apart from using a high-order discretization schema, no treatment of the present membrane locking is done [39]. We refer to [44], where a general strategy to avoid membrane locking is presented. For recent developments for the treatment of multi-patch geometries and the arising coupling constraints, we refer to [45–52].

In summary, the novelties of the present paper are (i) a parametrization-free formulation of the strong form of the governing equations of non-linear Kirchhoff–Love shells, (ii) the generation of manufactured solutions based on implicit surface descriptions for non-linear shells, and (iii) the application of the manufactured solutions in order-of-accuracy tests to IGA shell analysis. We remark that, due to the proposed approach of manufactured solutions based on implicit geometry descriptions, the suggested code verification can also be applied to other discretization methods for non-linear Kirchhoff–Love shells.

The remainder of this paper is structured as follows: In Section 2 we introduce our notation and discuss the geometry surfaces and differential operators on surfaces. The formulation of non-linear Kirchhoff–Love shells based on TDC is given in Section 3. In Section 4 IGA as discretization method for the Kirchhoff–Love shell problem is presented. The code verification procedure based on implicit surface representations is outlined in Section 5 and corresponding numerical results are given in Section 6. The paper concludes with a summary and an outlook in Section 7.

## 2. Notation and surface geometry

In this section we introduce our notation and review the geometry of surfaces for later use. We assume that the surface $\Omega \subset \mathbb{R}^3$ is regular (smooth) and oriented, *i.e.* a unit normal vector field $\boldsymbol{\nu} : \Omega \to S^2$ is given. In the following we are interested in derivatives of functions and tensor fields on $\Omega$. To this end we introduce $\nabla f$ as the usual gradient of some scalar-valued function $f : \mathbb{R}^3 \to \mathbb{R}$,

$$\nabla f(\mathbf{x}) = f_{,i}\, \mathbf{e}^i := \frac{\partial f(\mathbf{x})}{\partial x_i} \mathbf{e}^i \tag{1}$$

with the Cartesian coordinates $\mathbf{x} = (x_1, x_2, x_3)$ and the standard Cartesian orthonormal basis $\{\mathbf{e}^1, \mathbf{e}^2, \mathbf{e}^3\}$. Here, and in the following, the Einstein summation convention applies. Whenever an index occurs once in an upper position and in a lower position we sum over this index, where Latin indices $i, j, \dots$ take the values $1, 2, 3$ whereas Greek indices $\alpha, \beta, \dots$ take the values 1,2. Let $\mathcal{T}$ be some tensor space of the form $\mathbb{R}^3 \otimes \cdots \otimes \mathbb{R}^3$. In the following we also use the generalization of the gradient for scalar-valued functions (1) to tensor-valued functions $\mathbf{T} : \mathbb{R}^3 \to \mathcal{T}$,

$$\nabla \mathbf{T} = \mathbf{T}_{,i} \otimes \mathbf{e}^i. \tag{2}$$

**Remark 2.1.** In order to introduce the gradient of a scalar function (1) and a tensor field (2) we assumed global Cartesian coordinates on the *surrounding* space in order not to over-complicate the presentation. Nevertheless, in the following the equations are written in a coordinate-free way. We refer to [20] for a definition of the gradient also in a coordinate-free way.

By means of the normal vector we are able to define the tangential projector

$$\mathbf{P} = \mathbf{I} - \boldsymbol{\nu} \otimes \boldsymbol{\nu} \tag{3}$$

where $\mathbf{I}$ is the identity in $\mathbb{R}^3$. Now, the surface (tangential) gradient is defined by

$$\nabla_{\Omega}\mathbf{T} = \nabla\mathbf{T} \cdot \mathbf{P}. \tag{4}$$

We remark that in (4) we have assumed that $\mathbf{T}$ is defined over $\mathbb{R}^3$. However, in view of the deformation of shells we are mostly interested in the surface gradient of tensor fields defined on $\Omega$. Nevertheless, for $\bar{\mathbf{T}} : \Omega \to \mathcal{T}$ we are able to define by the closest point projection an extended field $\hat{\mathbf{T}} : \hat{\Omega} \to \mathcal{T}$ where $\hat{\Omega}$ is a three-dimensional tubular neighborhood of $\Omega$ such that (4) applies (see also [53]). In the following we do not fuss over this aspect and do not account for the extension in our notation. In order to measure curvature we introduce the curvature tensor (extended Weingarten map)

$$\mathbf{H} = -\nabla_{\Omega}\boldsymbol{\nu}. \tag{5}$$

The mean curvature $H$ is defined as

$$H = \mathrm{tr}_{\Omega}(\mathbf{H}) = \mathbf{H} : \mathbf{P}. \tag{6}$$

In the present paper, we define the double dot product of two tensors as the contraction of these tensors with respect to the last two indices of the first one, and the first two indices of the second one. The contraction is performed on the closest indices first, e.g.

$$\mathbf{A} : \mathbf{B} = \left(A_{ij}\mathbf{e}^i \otimes \mathbf{e}^j\right) : \left(B_{kl}\mathbf{e}^k \otimes \mathbf{e}^l\right) = A_{ij}B_{kl}(\mathbf{e}^j \cdot \mathbf{e}^k)(\mathbf{e}^i \cdot \mathbf{e}^l). \tag{7}$$

As a consequence we have

$$(\mathbf{A} \cdot \mathbf{B}) : \mathbf{C} = \mathbf{A} : (\mathbf{B} \cdot \mathbf{C}) = \mathbf{B} : (\mathbf{C} \cdot \mathbf{A}^{\top}). \tag{8}$$

As a next step, we define the surface (tangential) divergence as the adjoint operator to the surface gradient [54] and obtain, for the present situation [12]

$$\mathrm{div}\mathbf{T} = \nabla\mathbf{T} : \mathbf{P} + H\,\mathbf{T} \cdot \boldsymbol{\nu}. \tag{9}$$

For further use we introduce the surface divergence theorem for a tensor-valued function $\mathbf{T}$ [20]

$$\int_{\Omega} \mathrm{div}\,\mathbf{T}\,\mathrm{d}\mathbf{x} = \int_{\Gamma} \mathbf{T} \cdot \boldsymbol{\mu}\,\mathrm{d}s_{\mathbf{x}}. \tag{10}$$

Using the product rule for a vector $\mathbf{v}$ and a second order tensor $\mathbf{T}$,

$$\mathrm{div}(\mathbf{v} \cdot \mathbf{T}) = \mathbf{v} \cdot \mathrm{div}(\mathbf{T}) + \nabla_{\Omega}\mathbf{v} : \mathbf{T}^{\top}, \tag{11}$$

and (10), the integration by parts formula reads [20]

$$\int_{\Omega} \mathbf{v} \cdot \mathrm{div}\mathbf{T}\,\mathrm{d}\mathbf{x} = \int_{\Gamma} \mathbf{v} \cdot \mathbf{T} \cdot \boldsymbol{\mu}\,\mathrm{d}s_x - \int_{\Omega} \nabla_{\Omega}\mathbf{v} : \mathbf{T}^{\top}\,\mathrm{d}\mathbf{x}. \tag{12}$$

## 3. Theory of non-linear Kirchhoff–Love shells

In this section, we derive the governing equations of thin elastic shells under static loading from first principles of continuum mechanics [13,14]. To this end, we follow the direct approach, *i.e.* we use surface equilibrium equations. In principle these equations are known, however most of the literature uses local coordinates induced by a parametrization of the shell surface to formulate them. In contrast to this, in this section, the equations are written in direct notation and are formulated by means of tangential differential calculus.

### 3.1. Shell kinematics

In order to describe the kinematics of the deformation of a shell we distinguish between the initial configuration where the shell occupies the surface $\Omega$ and the current configuration which is denoted by $\omega$. The deformation $\boldsymbol{\varphi} : \Omega \to \omega$ is given by

$$\boldsymbol{\varphi}(\mathbf{X}) = \mathbf{X} + \mathbf{u}(\mathbf{X}), \tag{13}$$

where $\mathbf{u} : \Omega \to \mathbb{R}^3$ is the displacement vector field. In order to consider non-linear shell kinematics, we introduce the surface deformation gradient

$$\mathbf{F}(\mathbf{X}) = \nabla_{\Omega}\boldsymbol{\varphi}(\mathbf{X}) = \mathbf{P}(\mathbf{X}) + \nabla_{\Omega}\mathbf{u}(\mathbf{X}), \tag{14}$$

where $\mathbf{P}$ is the tangential projector of the initial configuration. With the pseudo-inverse of the deformation gradient $\mathbf{F}^{\dagger}$ it holds

$$\mathbf{P}(\mathbf{X}) = \mathbf{F}^{\dagger}(\mathbf{X}) \cdot \mathbf{F}(\mathbf{X}), \tag{15}$$

and the tangential projector of the current configuration $\bar{\mathbf{p}}(\mathbf{X}) = \mathbf{p}(\boldsymbol{\varphi}(\mathbf{X}))$ can be obtained by

$$\bar{\mathbf{p}}(\mathbf{X}) = \mathbf{F}(\mathbf{X}) \cdot \mathbf{F}^{\dagger}(\mathbf{X}). \tag{16}$$

In analogy to 3D continuum mechanics, we introduce the surface right Cauchy–Green tensor

$$\mathbf{C}(\mathbf{X}) = \mathbf{F}^{\top}(\mathbf{X})\mathbf{F}(\mathbf{X}), \tag{17}$$

and the surface Green–Lagrange deformation tensor

$$\mathbf{E}(\mathbf{X}) = \frac{1}{2}\left(\mathbf{C}(\mathbf{X}) - \mathbf{P}(\mathbf{X})\right). \tag{18}$$

Furthermore, the non-linear change in curvature tensor is defined by

$$\mathbf{K}(\mathbf{X}) = \mathbf{F}^{T}(\mathbf{X}) \cdot \mathbf{h}(\boldsymbol{\varphi}(\mathbf{X})) \cdot \mathbf{F}(\mathbf{X}) - \mathbf{H}(\mathbf{X}), \tag{19}$$

where the curvature tensor $\mathbf{h}$ of the deformed configuration is given by

$$\mathbf{h}(\mathbf{x}) = -\nabla_{\omega}\boldsymbol{\nu}(\mathbf{x}), \tag{20}$$

where $\boldsymbol{\nu}$ is the normal vector of the deformed configuration and $\mathbf{H}$ is the curvature tensor of the initial configuration. As the curvature tensor for the deformed configuration $\mathbf{h}(\mathbf{x})$ is not readily available in the implemented method, we recall the well-known change of variables formulas.

**Proposition 3.1.** *For a tensor $\mathbf{T} : \omega \to \mathcal{T}$ the change of variables formulas*

$$\nabla_{\Omega}(\mathbf{T}(\mathbf{x}) \circ \boldsymbol{\varphi}(\mathbf{X})) = (\nabla_{\omega}\mathbf{T}(\mathbf{x}) \circ \boldsymbol{\varphi}(\mathbf{X})) \cdot \mathbf{F}(\mathbf{X}) \tag{21}$$

*and*

$$(\nabla_{\omega}\mathbf{T}(\mathbf{x})) \circ \boldsymbol{\varphi}(\mathbf{X}) = \nabla_{\Omega}(\mathbf{T}(\mathbf{x}) \circ \boldsymbol{\varphi}(\mathbf{X})) \cdot \mathbf{F}^{\dagger}(\mathbf{X}) \tag{22}$$

*hold.*

Considering (21), we have

$$\bar{\mathbf{h}}(\mathbf{X}) := \mathbf{h}(\boldsymbol{\varphi}(\mathbf{X})) \cdot \mathbf{F}(\mathbf{X}) = -\left[\nabla_{\omega}\boldsymbol{\nu}(\mathbf{x}) \circ \boldsymbol{\varphi}(\mathbf{X})\right] \cdot \mathbf{F}(\mathbf{X}) = -\nabla_{\Omega}\boldsymbol{\nu}(\boldsymbol{\varphi}(\mathbf{X})), \tag{23}$$

where the rightmost expression is computationally available and thus the change in curvature tensor can be written as

$$\mathbf{K}(\mathbf{X}) = \mathbf{F}^{T}(\mathbf{X}) \cdot \bar{\mathbf{h}}(\mathbf{X}) - \mathbf{H}(\mathbf{X}). \tag{24}$$

We note that the vector field $\bar{\boldsymbol{\nu}}(\mathbf{X}) = \boldsymbol{\nu}(\boldsymbol{\varphi}(\mathbf{X}))$ is given by

$$\bar{\boldsymbol{\nu}}(\mathbf{X}) = \frac{1}{J(\mathbf{X})}\operatorname{cof}\mathbf{F}(\mathbf{X}) \cdot \boldsymbol{\nu}_0(\mathbf{X}) \tag{25}$$

where $\operatorname{cof}\mathbf{F}$ denotes the co-factor matrix of $\mathbf{F}$, $\boldsymbol{\nu}_0$ the normal vector of the initial configuration and $J$ which is related to the change in surface area is given by

$$J(\mathbf{X}) = |\operatorname{cof}\mathbf{F}(\mathbf{X}) \cdot \boldsymbol{\nu}_0(\mathbf{X})|. \tag{26}$$

We remark that the three invariants of the surface right Cauchy–Green tensor are given by

$$I_1 = \operatorname{tr}(\mathbf{C}), \tag{27a}$$

$$I_2 = \frac{1}{2}\left((\operatorname{tr}(\mathbf{C}))^2 - \operatorname{tr}(\mathbf{C} \cdot \mathbf{C})\right), \tag{27b}$$

$$I_3 = \det(\mathbf{C}) = 0, \tag{27c}$$

and observe the relation $I_2 = J^2$.

### 3.2. Stress and moment tensors

We introduce the Cauchy traction vector $\mathbf{t}_{\sigma}(\mathbf{x})$ at $\mathbf{x} \in \omega$ on a cut normal to the vector $\boldsymbol{\mu}(\mathbf{x})$, which is tangential to the surface. Due to Cauchy's theorem, we have the representation

$$\mathbf{t}_{\sigma}(\mathbf{x}) = \boldsymbol{\sigma}(\mathbf{x}) \cdot \boldsymbol{\mu}(\mathbf{x}), \tag{28}$$

with the Cauchy stress tensor $\boldsymbol{\sigma}$. We decompose the Cauchy stress tensor $\boldsymbol{\sigma}$ in a tangential and a normal part,

$$\boldsymbol{\sigma}(\mathbf{x}) = \mathbf{n}(\mathbf{x}) + \boldsymbol{\nu}(\mathbf{x}) \otimes \mathbf{s}(\mathbf{x}), \tag{29}$$

with the tangential membrane stress tensor $\mathbf{n} = \mathbf{p} \cdot \mathbf{n} \cdot \mathbf{p}$ and the tangential vector $\mathbf{s} = \mathbf{p} \cdot \mathbf{s}$ related to transverse shear. Analogously, we have a Cauchy moment vector $\mathbf{t}_m(\mathbf{x})$ on the cut normal to the vector $\boldsymbol{\mu}$, which can be expressed as

$$\mathbf{t}_m(\mathbf{x}) = \boldsymbol{\nu}(\mathbf{x}) \times (\mathbf{m}(\mathbf{x}) \cdot \boldsymbol{\mu}(\mathbf{x})), \tag{30}$$

by means of the tangential moment tensor $\mathbf{m} = \mathbf{p} \cdot \mathbf{m} \cdot \mathbf{p}$.

### 3.3. Equilibrium of forces

The equilibrium of forces states that the sum of the resulting force of boundary traction and the resultant force from the surface loading vanishes,

$$\int_\gamma \mathbf{t}_\sigma(\mathbf{x})\, \mathrm{d}s_\mathbf{x} + \int_\omega \mathbf{b}(\mathbf{x})\, \mathrm{d}\mathbf{x} = \mathbf{0}, \tag{31}$$

where $\mathbf{b}$ is the current surface load per area. Applying the surface divergence theorem (10), results in

$$\int_\omega \mathrm{div}_\omega\, \boldsymbol{\sigma}(\mathbf{x}) + \mathbf{b}(\mathbf{x})\, \mathrm{d}\mathbf{x} = \mathbf{0}. \tag{32}$$

Due to the fact that $\Omega$ is arbitrary, the local force equilibrium in the current configuration reads

$$\mathrm{div}_\omega\, \boldsymbol{\sigma}(\mathbf{x}) + \mathbf{b}(\mathbf{x}) = \mathbf{0}. \tag{33}$$

The local force equilibrium in the initial configuration and the surface Piola transformation are given in the next theorem.

**Lemma 3.2.** *Provided that the first Piola–Kirchhoff surface stress tensor is given by the surface Piola transformation*

$$^I\mathbf{N}(\mathbf{X}) = J(\mathbf{X})\boldsymbol{\sigma}(\varphi(\mathbf{X}))\cdot \mathbf{F}^\dagger(\mathbf{X})^\top, \tag{34}$$

*then*

$$\mathrm{div}_\Omega\, ^I\mathbf{N}(\mathbf{X}) = J(\mathbf{X})\mathrm{div}_\omega(\boldsymbol{\sigma}(\mathbf{x}))\circ\boldsymbol{\varphi}(\mathbf{X}). \tag{35}$$

*Furthermore, the local form of the equilibrium in the initial configuration reads*

$$\mathrm{div}_\Omega\, ^I\mathbf{N}(\mathbf{X}) + \mathbf{B}(\mathbf{X}) = 0, \tag{36}$$

*where* $\mathbf{B}(\mathbf{X}) = \mathbf{b}(\varphi(\mathbf{X}))J(\mathbf{X})$.

A proof of Lemma 3.2 can be found in Appendix A.1.

**Remark 3.3.** Relation (34) can be considered as the surface Piola transformation and it generalizes the classical Piola transformation

$$^I\mathbf{N} = J\boldsymbol{\sigma}\cdot\mathbf{F}^{-\top} = \boldsymbol{\sigma}\cdot\mathrm{cof}\,\mathbf{F} \tag{37}$$

where $\mathbf{F}$ has to be invertible. A proof of (35) relying on the identity

$$\mathrm{div}\,\mathrm{cof}\,\mathbf{F} = \mathbf{0} \tag{38}$$

and thus on the invertibility of $\mathbf{F}$ can be found, for example in [55,56]. We remark that (38) holds true also in the case of surfaces [57].

**Corollary 3.4.** *Due to the divergence theorem, (35) implies the identities [56, Theorem 1.7-1]*

$$\int_\gamma \boldsymbol{\sigma}(\mathbf{x})\cdot\boldsymbol{\mu}(\mathbf{x})\, \mathrm{d}s_\mathbf{x} = \int_\Gamma {}^I\mathbf{N}(\mathbf{X})\cdot\boldsymbol{\mu}_0(\mathbf{X})\, \mathrm{d}s_\mathbf{X}, \tag{39}$$

*and*

$$\int_\gamma \mathbf{v}(\mathbf{x})\cdot\boldsymbol{\sigma}(\mathbf{x})\cdot\boldsymbol{\mu}(\mathbf{x})\, \mathrm{d}s_\mathbf{x} = \int_\Gamma \mathbf{v}(\boldsymbol{\varphi}(\mathbf{X}))\cdot {}^I\mathbf{N}(\mathbf{X})\cdot\boldsymbol{\mu}_0(\mathbf{X})\, \mathrm{d}s_\mathbf{X} \tag{40}$$

*where* $\mathbf{v}(\mathbf{x})$ *is an arbitrary vector field.*

### 3.4. Equilibrium of moments

The equilibrium of moments states that the sum of boundary moments, the moments of boundary tractions and the moments due to surface loads vanishes,

$$\int_\gamma \mathbf{t}_m(\mathbf{x}) + \mathbf{x}\times\mathbf{t}_\sigma(\mathbf{x})\, \mathrm{d}s_x + \int_\omega \mathbf{x}\times\mathbf{b}(\mathbf{x})\, \mathrm{d}\mathbf{x} = \mathbf{0}. \tag{41}$$

The following lemma summarizes the consequences of the equilibrium of moments.

**Lemma 3.5.** *For* $\mathbf{T} = T_{ij}\mathbf{e}^i\otimes\mathbf{e}^j$ *let* $[\mathbf{T}]_\times = T_{ij}\mathbf{e}^i\times\mathbf{e}^j$. *The equilibrium of moments is fulfilled if*

$$[-\mathbf{h}(\mathbf{x})\cdot\mathbf{m}(\mathbf{x}) + \mathbf{n}(\mathbf{x})^\top]_\times = \mathbf{0}, \tag{42}$$

*and*

$$\mathbf{s}(\mathbf{x}) = \mathbf{P}_t(\mathbf{x})\cdot\mathrm{div}_\omega\mathbf{m}(\mathbf{x}). \tag{43}$$

A proof of Lemma 3.5 can be found in [12]. In view of Lemma 3.5, we assume that the Cauchy stress tensor $\boldsymbol{\sigma}$ can be expressed by

$$\boldsymbol{\sigma}(\mathbf{x}) = \bar{\mathbf{n}}(\mathbf{x}) - \mathbf{h}(\mathbf{x}) \cdot \mathbf{m}(\mathbf{x}) + \boldsymbol{\nu}(\mathbf{x}) \otimes (\mathbf{P}_t(\mathbf{x}) \cdot \operatorname{div}_\omega \mathbf{m}(\mathbf{x})) \tag{44}$$

where $\bar{\mathbf{n}}(\mathbf{x})$ and $\mathbf{m}(\mathbf{x})$ are constitutively determinate.

### 3.5. Mechanical power

In order to formulate constitutive equations, it is favorable to derive the mechanical power. To this end, although not explicitly stated, we assume in the following a time dependency of all quantities and denote the time derivative of by $\dot{(\,)}$. In the following lemma the mechanical power in the current as well as in the initial configuration is given.

**Lemma 3.6.** *Let* $\mathbf{v}(\mathbf{x})$ *be the velocity implicitly defined by*

$$\mathbf{v}(\boldsymbol{\varphi}(\mathbf{X})) = \dot{\boldsymbol{\varphi}}(\mathbf{X}), \tag{45}$$

$\mathbf{d}(\mathbf{x}) = \mathbf{p}(\mathbf{x}) \cdot \operatorname{sym} \nabla_\omega \mathbf{v}(\mathbf{x}) \cdot \mathbf{p}(\mathbf{x})$ *the tangential and symmetric part of the velocity gradient and* $\mathbf{k}(\mathbf{x}) = \boldsymbol{\nu}(\mathbf{x}) \cdot \nabla_\omega \nabla_\omega \mathbf{v}(\mathbf{x})$. *Then, the mechanical power formulated in the current configuration*

$$\int_\omega \mathbf{d} : \bar{\mathbf{n}} - \mathbf{k} : \mathbf{m} \, \mathrm{d}\mathbf{x} = \int_\omega \mathbf{v} \cdot \mathbf{b} \, \mathrm{d}\mathbf{x} + \int_\gamma \mathbf{v} \cdot \boldsymbol{\sigma} \cdot \boldsymbol{\mu} \, \mathrm{d}s_{\mathbf{x}} - \int_\gamma \boldsymbol{\nu} \cdot \nabla_\omega \mathbf{v} \cdot \mathbf{m} \cdot \boldsymbol{\mu} \, \mathrm{d}s_{\mathbf{x}}, \tag{46}$$

*follows from the equilibrium equations. Furthermore, let* ${}^{II}\bar{\mathbf{N}}$ *be the second Piola–Kirchhoff surface membrane-stress tensor given by*

$${}^{II}\bar{\mathbf{N}}(\mathbf{X}) = \mathbf{F}^\dagger(\mathbf{X}) \cdot \bar{\mathbf{n}}(\varphi(\mathbf{X})) \cdot \mathbf{F}^\dagger(\mathbf{X})^\top J(\mathbf{X}), \tag{47}$$

*and* ${}^{II}\mathbf{M}$ *be the second Piola–Kirchhoff surface moment tensor given by*

$${}^{II}\mathbf{M}(\mathbf{X}) = \mathbf{F}^\dagger(\mathbf{X}) \cdot \mathbf{m}(\varphi(\mathbf{X})) \cdot \mathbf{F}^\dagger(\mathbf{X})^\top J(\mathbf{X}). \tag{48}$$

*Then, the mechanical power in the reference configuration reads*

$$\begin{aligned} \int_\Omega \dot{\mathbf{E}} : {}^{II}\bar{\mathbf{N}} - \dot{\mathbf{K}} : {}^{II}\mathbf{M} \, \mathrm{d}\mathbf{X} &= \int_\Omega \mathbf{V} \cdot \mathbf{B} \, \mathrm{d}\mathbf{X} \\ &+ \int_\Gamma \mathbf{V} \cdot {}^{I}\mathbf{N} \cdot \boldsymbol{\mu}_0 \, \mathrm{d}s_{\mathbf{X}} + \int_\Gamma \dot{\mathbf{v}} \cdot {}^{I}\mathbf{M} \cdot \boldsymbol{\mu}_0 \, \mathrm{d}s_{\mathbf{X}}, \end{aligned} \tag{49}$$

*where* $\mathbf{V}(\mathbf{X}) = \mathbf{v}(\varphi(\mathbf{X})) = \dot{\boldsymbol{\varphi}}(\mathbf{X})$.

A proof of Lemma 3.6 can be found in Appendix A.2.

### 3.6. Constitutive equations

In view of Lemma 3.6, we assume in the present paper linear constitutive equations of the form

$${}^{II}\mathbf{M} = -\frac{t^3}{12} \mathbb{C} : \mathbf{K}, \tag{50}$$

and

$${}^{II}\bar{\mathbf{N}} = t \, \mathbb{C} : \mathbf{E}, \tag{51}$$

where $t$ denotes the thickness of the shell. Here, the fourth order surface elasticity tensor $\mathbb{C}$ incorporating the plane stress assumption is given by

$$\mathbb{C} = \bar{\lambda}(\mathbf{P} \otimes \mathbf{P}) + 2\mu \mathcal{P}^s, \qquad \text{with} \quad \lambda = \frac{4\lambda\mu}{\lambda + 2\mu}, \tag{52}$$

where $\lambda$ and $\mu$ are the Lamé constants of the elastic material constituting the shell and $\mathcal{P}^s$ the symmetric part of the tangential fourth order identity tensor. The Lamé constants are related to the Young's modulus $E > 0$ and Poisson's ratio $0 \le \nu \le \frac{1}{2}$ by

$$\lambda = \frac{E\nu}{(1+\nu)(1-2\nu)}, \qquad \mu = \frac{E}{2(1+\nu)}. \tag{53}$$

The constitutive equations can also be written as

$${}^{II}\mathbf{N} = {}^{II}\bar{\mathbf{N}} - \mathbf{F}^\dagger \cdot \hat{\mathbf{h}} \cdot {}^{II}\mathbf{M} \quad \text{with} \quad {}^{II}\bar{\mathbf{N}} = t(\lambda \, \mathbf{P} \operatorname{tr} \mathbf{E} + 2\mu \, \mathbf{E}), \tag{54a}$$

$${}^{II}\mathbf{M} = -\frac{t^3}{12}(\lambda \, \mathbf{P} \operatorname{tr} \mathbf{K} + 2\mu \, \mathbf{K}), \tag{54b}$$

and, furthermore, we have

$${}^{I}\mathbf{N} = \mathbf{F} \cdot {}^{II}\bar{\mathbf{N}} - \hat{\mathbf{h}} \cdot {}^{II}\mathbf{M}, \tag{55a}$$

$${}^{I}\mathbf{M} = -\frac{t^3}{12}(\lambda \, \mathbf{F} \operatorname{tr} \mathbf{K} + 2\mu \, \mathbf{F} \cdot \mathbf{K}). \tag{55b}$$

### 3.7. Weak form of the governing equations

Let $\delta\mathbf{u}$ be the virtual displacement, $\mathcal{E}(\mathbf{u},\delta\mathbf{u})$ be the variation of $\mathbf{E}(\mathbf{u})$ defined by

$$\mathcal{E}(\mathbf{u},\delta\mathbf{u}) = \left[\frac{d}{d\alpha}\mathbf{E}(\mathbf{u}+\alpha\delta\mathbf{u})\right]_{\alpha=0}, \tag{56}$$

and $\boldsymbol{\mathcal{K}}(\mathbf{u},\delta\mathbf{u})$ the variation of $\mathbf{K}(\mathbf{u})$. The weak form of the governing equations for the reference configuration reads

$$R_{int}(\mathbf{u},\delta\mathbf{u}) - R_{ext}(\mathbf{u},\delta\mathbf{u}) = 0 \tag{57}$$

with

$$R_{int}(\mathbf{u},\delta\mathbf{u}) = \int_\Omega \mathcal{E}(\mathbf{u},\delta\mathbf{u}) : {}^{II}\bar{\mathbf{N}}(\mathbf{u}) - \mathcal{K}(\mathbf{u},\delta\mathbf{u}) : {}^{II}\mathbf{M}(\mathbf{u})\,\mathrm{d}\mathbf{X},$$
$$R_{ext}(\mathbf{u},\delta\mathbf{u}) = \int_\Omega \delta\mathbf{u}\cdot\mathbf{B}\,\mathrm{d}\mathbf{X} + \int_{\Gamma_\sigma}\delta\mathbf{u}\cdot\mathbf{T}^*_\sigma\,\mathrm{d}s_\mathbf{X} + \int_{\Gamma_m}(\delta\bar{\boldsymbol{\nu}}\times\bar{\boldsymbol{\nu}})\cdot\mathbf{T}^*_m\,\mathrm{d}s_\mathbf{X},$$

where on the Neumann boundaries $\Gamma_\sigma$ and $\Gamma_m$ the traction vector $\mathbf{T}^*_\sigma$ and the moment vector $\mathbf{T}^*_m$ are prescribed, respectively. Here, we assumed that $\mathbf{T}^*_\sigma$ and $\mathbf{T}^*_m$ are related to $\mathbf{t}^*_\sigma$ and $\mathbf{t}^*_m$ by

$$\mathbf{T}^*_\sigma = \frac{\mathbf{t}^*_\sigma}{\|\mathbf{F}\boldsymbol{\tau}\|}, \quad \mathbf{T}^*_m = \frac{\mathbf{t}^*_m}{\|\mathbf{F}\boldsymbol{\tau}\|},$$

where $\boldsymbol{\tau}$ is the tangent vector to the boundary $\Gamma$. The Dirichlet boundary conditions which are assumed to be fulfilled in a strong sense are $\mathbf{u}=\mathbf{u}^*$ on $\Gamma\setminus\Gamma_\sigma$ and $\bar{\boldsymbol{\nu}}(\mathbf{u})=\boldsymbol{\nu}^*$ on $\Gamma\setminus\Gamma_m$ with prescribed functions $\mathbf{u}^*$ and $\boldsymbol{\nu}^*$. The derivation of (57) is analogously to the proof of the mechanical power balance in Lemma 3.6 by replacing the velocity $\mathbf{V}(\mathbf{X})$ by the virtual displacement $\delta\mathbf{u}$ and taking into account that $\delta\mathbf{u}$ is restricted to functions such that the arising boundary integrals over Dirichlet boundary parts vanish. For simplicity, we assume $\Gamma_m=\Gamma$ in the rest of the paper.

## 4. Isogeometric discretization

In IGA it is assumed that the initial surface $\Omega$ is defined by a parametrization $\mathfrak{G} : U\subset\mathbb{R}^2\to\Omega$ with the parameter plane $U=[0,1]^2$ and that $\mathfrak{G}$ is realized by splines. For details on IGA and splines we refer to [58,59]. Thus, in the following of this section, we only review the differential geometry of parametrized surfaces and give all necessary quantities along with their variation and linearization in order to be able to implement the method.

### 4.1. Differential geometry of parametrized surfaces

We briefly review the differential geometry of parametrized surfaces. For details we refer to e.g. [60]. Given the parametrization $\mathfrak{G}(\boldsymbol{\theta})$, we can define the two covariant base vectors $\hat{\mathbf{G}}_\alpha := \frac{\partial\mathfrak{G}}{\partial\theta^\alpha}$, which span the tangent plane to $\Omega$. With the base vectors we can compute the surface normal vector

$$\hat{\boldsymbol{\nu}}_0(\boldsymbol{\theta}) = \frac{\hat{\mathbf{G}}_1(\boldsymbol{\theta})\times\hat{\mathbf{G}}_2(\boldsymbol{\theta})}{\|\hat{\mathbf{G}}_1(\boldsymbol{\theta})\times\hat{\mathbf{G}}_2(\boldsymbol{\theta})\|}, \tag{58}$$

and the covariant coefficients of the metric $\hat{G}_{\alpha\beta}=\hat{\mathbf{G}}_\alpha\cdot\hat{\mathbf{G}}_\beta$. The contravariant coefficients of the metric are given by $[\hat{G}^{\alpha\beta}]=[\hat{G}_{\alpha\beta}]^{-1}$, where $[\hat{G}_{\alpha\beta}]$ is the coefficient matrix. The contravariant base vectors can then be computed by $\hat{\mathbf{G}}^\alpha=\hat{G}^{\alpha\beta}\hat{\mathbf{G}}_\beta$. The covariant coefficients of the curvature tensor $\hat{\mathbf{H}}=\hat{H}_{\alpha\beta}\hat{\mathbf{G}}^\alpha\otimes\hat{\mathbf{G}}^\beta$ are given by

$$\hat{H}_{\alpha\beta} = -\hat{\mathbf{G}}_\alpha\cdot\hat{\boldsymbol{\nu}}_{0,\beta} = \hat{\mathbf{G}}_{\alpha,\beta}\cdot\hat{\boldsymbol{\nu}}_0, \tag{59}$$

and obey the symmetry relation $\hat{H}_{\alpha\beta}=\hat{H}_{\beta\alpha}$. The mean curvature $\hat{H}$ is given by

$$\hat{H} = \hat{H}^\alpha_\alpha = \hat{H}_{\alpha\beta}\hat{G}^{\beta\alpha}. \tag{60}$$

Furthermore, the derivatives of the base vectors are given by

$$\begin{aligned}\hat{\mathbf{G}}_{\alpha,\beta} &= \Gamma^\gamma_{\alpha\beta}\hat{\mathbf{G}}_\gamma + \hat{H}_{\alpha\beta}\hat{\boldsymbol{\nu}}_0,\\ \hat{\mathbf{G}}^\alpha_{,\beta} &= -\Gamma^\alpha_{\beta\gamma}\hat{\mathbf{G}}^\gamma + \hat{H}^\alpha_\beta\hat{\boldsymbol{\nu}}_0,\end{aligned} \tag{61}$$

with the surface Christoffel symbols of the second kind defined by

$$\Gamma^\gamma_{\alpha\beta} = \hat{\mathbf{G}}^\gamma\cdot\hat{\mathbf{G}}_{\alpha,\beta}. \tag{62}$$

The surface gradient of a tensor field $\mathbf{T}:\Omega\to\mathcal{T}$ is given by

$$(\nabla_\Omega\mathbf{T})\circ\mathfrak{G}(\boldsymbol{\theta}) = (\mathbf{T}\circ\mathfrak{G}(\boldsymbol{\theta}))_{,\alpha}\otimes\hat{\mathbf{G}}^\alpha = \hat{\mathbf{T}}(\boldsymbol{\theta})_{,\alpha}\otimes\hat{\mathbf{G}}^\alpha, \tag{63}$$

whereas the surface divergence reads

$$(\mathrm{div}\mathbf{T})\circ\mathfrak{G}(\boldsymbol{\theta}) = (\mathbf{T}\circ\mathfrak{G}(\boldsymbol{\theta}))_{,\alpha}\cdot\hat{\mathbf{g}}^\alpha + \hat{H}\,(\mathbf{T}\circ\mathfrak{G}(\boldsymbol{\theta}))\cdot\hat{\boldsymbol{\nu}}_0. \tag{64}$$

The deformed configuration is described by the parametrization

$$\mathfrak{g}(\boldsymbol{\theta}) = \mathfrak{G}(\boldsymbol{\theta}) + \hat{\mathbf{u}}(\boldsymbol{\theta}), \tag{65}$$

which induces the base vectors $\hat{\mathbf{g}}_\alpha$ and $\hat{\mathbf{g}}^\alpha$ analogously to the initial configuration. In local coordinates we have for the deformation gradient

$$\hat{\mathbf{F}}(\boldsymbol{\theta}) = \hat{\mathbf{g}}_\alpha(\boldsymbol{\theta}) \otimes \hat{\mathbf{G}}^\alpha(\boldsymbol{\theta}), \tag{66a}$$

$$\hat{\mathbf{F}}^\top(\boldsymbol{\theta}) = \hat{\mathbf{G}}^\alpha(\boldsymbol{\theta}) \otimes \hat{\mathbf{g}}_\alpha(\boldsymbol{\theta}), \tag{66b}$$

$$\hat{\mathbf{F}}^\dagger(\boldsymbol{\theta}) = \hat{\mathbf{G}}_\alpha(\boldsymbol{\theta}) \otimes \hat{\mathbf{g}}^\alpha(\boldsymbol{\theta}), \tag{66c}$$

$$\hat{\mathbf{F}}^{\dagger\top}(\boldsymbol{\theta}) = \hat{\mathbf{g}}^\alpha(\boldsymbol{\theta}) \otimes \hat{\mathbf{G}}_\alpha(\boldsymbol{\theta}). \tag{66d}$$

Therefore, we have

$$\hat{\mathbf{P}}(\boldsymbol{\theta}) = \hat{\mathbf{F}}^\dagger(\boldsymbol{\theta}) \cdot \hat{\mathbf{F}}(\boldsymbol{\theta}) = \hat{\mathbf{G}}_\alpha(\boldsymbol{\theta}) \otimes \hat{\mathbf{G}}^\alpha(\boldsymbol{\theta}) = \hat{G}_{\alpha\beta}(\boldsymbol{\theta})\, \hat{\mathbf{G}}^\alpha(\boldsymbol{\theta}) \otimes \hat{\mathbf{G}}^\beta(\boldsymbol{\theta}), \tag{67}$$

and obtain for the surface Green–Lagrange deformation tensor

$$\hat{\mathbf{E}}(\boldsymbol{\theta}) = \frac{1}{2}\left(\hat{g}_{\alpha\beta}(\boldsymbol{\theta}) - \hat{G}_{\alpha\beta}(\boldsymbol{\theta})\right) \hat{\mathbf{G}}^\alpha(\boldsymbol{\theta}) \otimes \hat{\mathbf{G}}^\beta(\boldsymbol{\theta}), \tag{68}$$

where $\hat{g}_{\alpha\beta}(\boldsymbol{\theta}) = \hat{\mathbf{g}}_\alpha(\boldsymbol{\theta}) \cdot \hat{\mathbf{g}}_\beta(\boldsymbol{\theta})$ are the covariant coefficients of the metric for the deformed surface. For the change in curvature tensor we have

$$\hat{\mathbf{K}}(\boldsymbol{\theta}) = \left(\hat{h}_{\alpha\beta}(\boldsymbol{\theta}) - \hat{H}_{\alpha\beta}(\boldsymbol{\theta})\right) \hat{\mathbf{G}}^\alpha(\boldsymbol{\theta}) \otimes \hat{\mathbf{G}}^\beta(\boldsymbol{\theta}), \tag{69}$$

where $\hat{h}_{\alpha\beta}(\boldsymbol{\theta}) = \hat{\mathbf{g}}_{\alpha,\beta}(\boldsymbol{\theta}) \cdot \hat{\boldsymbol{\nu}}(\boldsymbol{\theta})$ are the covariant coefficients of the curvature tensor of the deformed surface. The surface elasticity tensor $\mathbb{C}$ in local coordinates is given by

$$\hat{\mathbb{C}} = \left(\bar{\lambda}\hat{G}^{\alpha\beta}\hat{G}^{\gamma\varphi} + \mu(\hat{G}^{\alpha\gamma}\hat{G}^{\beta\varphi} + \hat{G}^{\alpha\varphi}\hat{G}^{\beta\gamma})\right) \hat{\mathbf{G}}_\alpha \otimes \hat{\mathbf{G}}_\beta \otimes \hat{\mathbf{G}}_\gamma \otimes \hat{\mathbf{G}}_\varphi. \tag{70}$$

### 4.2. Governing equations and linearization for parametrized surfaces

In this section, we provide the variations and linearizations of all quantities necessary to implement the isogeometric discretization of the given problem. We are interested in the internal virtual work

$$\hat{R}_{int}(\hat{\mathbf{u}}, \delta\hat{\mathbf{u}}) = \int_U \left( t\hat{\mathbf{E}}(\hat{\mathbf{u}}) : \hat{\mathbb{C}} : \hat{\mathcal{E}}(\hat{\mathbf{u}}, \delta\hat{\mathbf{u}}) + \frac{t^3}{12}\hat{\mathbf{K}}(\hat{\mathbf{u}}) : \hat{\mathbb{C}} : \hat{\mathcal{K}}(\hat{\mathbf{u}}, \delta\hat{\mathbf{u}}) \right) \hat{J}\, \mathrm{d}\theta, \tag{71}$$

with $\hat{J} = \sqrt{\det[\hat{G}_{\alpha\beta}]}$ and the external virtual work

$$\hat{R}_{ext}(\hat{\mathbf{u}}, \delta\hat{\mathbf{u}}) = \int_U \hat{\mathbf{B}} \cdot \delta\hat{\mathbf{u}} \hat{J}\, \mathrm{d}\theta + \int_{\partial U_\sigma} \delta\hat{\mathbf{u}} \cdot \hat{\mathbf{T}}^*_\sigma \hat{J}_b\, \mathrm{d}s_\theta + \int_{\partial U_m} (\delta\hat{\boldsymbol{\nu}} \times \hat{\boldsymbol{\nu}}) \cdot \hat{\mathbf{T}}^*_m \hat{J}_b\, \mathrm{d}s_\theta \tag{72}$$

where $\hat{J}_b$ is the length of the base vector along the boundary $\partial U$. The variation of the covariant base vectors and the covariant metric coefficients are

$$\delta\hat{\mathbf{g}}_\alpha(\hat{\mathbf{u}}, \delta\hat{\mathbf{u}}) = \delta\hat{\mathbf{u}}_{,\alpha}, \tag{73}$$

$$\delta\hat{g}_{\alpha\beta}(\hat{\mathbf{u}}, \delta\hat{\mathbf{u}}) = \delta\hat{\mathbf{u}}_{,\alpha} \cdot \hat{\mathbf{g}}_\beta(\hat{\mathbf{u}}) + \hat{\mathbf{g}}_\alpha(\hat{\mathbf{u}}) \cdot \delta\hat{\mathbf{u}}_{,\beta}. \tag{74}$$

Therefore, the variation of the surface Green–Lagrange deformation tensor (68) is

$$\hat{\mathcal{E}}(\hat{\mathbf{u}}, \delta\hat{\mathbf{u}}) = \frac{1}{2}\left(\delta\hat{\mathbf{u}}_{,\alpha} \cdot \hat{\mathbf{g}}_\beta(\hat{\mathbf{u}}) + \hat{\mathbf{g}}_\alpha(\hat{\mathbf{u}}) \cdot \delta\hat{\mathbf{u}}_{,\beta}\right) \hat{\mathbf{G}}^\alpha \otimes \hat{\mathbf{G}}^\beta. \tag{75}$$

For the variation of change in curvature tensor the variation of the normal vector is needed. For later use we give also the variation of the contravariant base vectors in the next Lemma.

**Lemma 4.1.** *The variation of the normal vector reads [1]*

$$\delta\hat{\boldsymbol{\nu}}(\hat{\mathbf{u}}, \delta\hat{\mathbf{u}}) = -\hat{\mathbf{g}}^\alpha(\hat{\mathbf{u}})\left(\delta\hat{\mathbf{u}}_{,\alpha} \cdot \hat{\boldsymbol{\nu}}(\hat{\mathbf{u}})\right), \tag{76}$$

*and the variation of the contravariant base vectors is*

$$\delta\hat{\mathbf{g}}^\alpha(\hat{\mathbf{u}}, \delta\hat{\mathbf{u}}) = \left(g^{\alpha\beta}(\hat{\mathbf{u}})\hat{\boldsymbol{\nu}}(\hat{\mathbf{u}}) \otimes \hat{\boldsymbol{\nu}}(\hat{\mathbf{u}}) - \hat{\mathbf{g}}^\beta(\hat{\mathbf{u}}) \otimes \hat{\mathbf{g}}^\alpha(\hat{\mathbf{u}})\right) \cdot \delta\hat{\mathbf{u}}_{,\beta}. \tag{77}$$

Proofs of Lemma 4.1 based on direct calculations can be found for example in [1,61]. In Appendix A.3 we provide an alternative proof. Using the result (76) the variation of the change in curvature tensor (69) then gives [14,60]

$$\hat{\mathcal{K}}(\hat{\mathbf{u}},\delta\hat{\mathbf{u}}) = \left[\delta\hat{\mathbf{v}}(\hat{\mathbf{u}},\delta\hat{\mathbf{u}})\cdot\hat{\mathbf{g}}_{\alpha,\beta}(\hat{\mathbf{u}}) + \hat{\mathbf{v}}(\hat{\mathbf{u}})\cdot\delta\hat{\mathbf{u}}_{,\alpha\beta}\right]\hat{\mathbf{G}}^{\alpha}\otimes\hat{\mathbf{G}}^{\beta} \tag{78}$$

$$= \left[\hat{\mathbf{v}}(\hat{\mathbf{u}})\cdot(\delta\hat{\mathbf{u}}_{,\alpha\beta} - \Gamma^{\gamma}_{\alpha\beta}(\hat{\mathbf{u}})\delta\hat{\mathbf{u}}_{,\gamma})\right]\hat{\mathbf{G}}^{\alpha}\otimes\hat{\mathbf{G}}^{\beta}. \tag{79}$$

In the following we are interested in the linearization of the virtual work, which yields the tangent matrix needed in Newton's method. The linearization of the internal virtual work reads

$$LR^{int}_{(\hat{\mathbf{u}},\delta\hat{\mathbf{u}})}(\Delta\hat{\mathbf{u}}) = R_{int}(\hat{\mathbf{u}},\delta\hat{\mathbf{u}}) + \Delta R^{int}_{(\hat{\mathbf{u}},\delta\hat{\mathbf{u}})}(\Delta\hat{\mathbf{u}})$$

with

$$\begin{aligned}\Delta R^{int}_{(\hat{\mathbf{u}},\delta\hat{\mathbf{u}})}(\Delta\hat{\mathbf{u}}) = t\int_{\Omega}\hat{\mathcal{E}}(\hat{\mathbf{u}},\Delta\hat{\mathbf{u}}) : \hat{\mathbb{C}} : \hat{\mathcal{E}}(\hat{\mathbf{u}},\delta\hat{\mathbf{u}}) + \hat{\mathbf{E}}(\hat{\mathbf{u}}) : \hat{\mathbb{C}} : \Delta\hat{\mathcal{E}}_{(\hat{\mathbf{u}},\delta\hat{\mathbf{u}})}(\Delta\hat{\mathbf{u}})\,\mathrm{d}\mathbf{X}\\ + \frac{t^3}{12}\int_{\Omega}\hat{\mathcal{K}}(\hat{\mathbf{u}},\delta\hat{\mathbf{u}}) : \hat{\mathbb{C}} : \hat{\mathcal{K}}(\hat{\mathbf{u}},\Delta\hat{\mathbf{u}}) + \hat{\mathbf{K}}(\hat{\mathbf{u}}) : \hat{\mathbb{C}} : \Delta\hat{\boldsymbol{\mathcal{K}}}_{(\hat{\mathbf{u}},\delta\hat{\mathbf{u}})}(\Delta\hat{\mathbf{u}})\,\mathrm{d}\mathbf{X},\end{aligned} \tag{80}$$

where we used

$$\Delta\hat{\mathbf{E}}_{(\hat{\mathbf{u}})}(\Delta\hat{\mathbf{u}}) = \hat{\mathcal{E}}(\hat{\mathbf{u}},\Delta\hat{\mathbf{u}}),$$
$$\Delta\hat{\mathbf{K}}_{(\hat{\mathbf{u}})}(\Delta\hat{\mathbf{u}}) = \hat{\mathcal{K}}(\hat{\mathbf{u}},\Delta\hat{\mathbf{u}}).$$

For the derivative of the variation of the surface Green–Lagrange deformation tensor we have

$$\Delta\hat{\mathcal{E}}_{(\hat{\mathbf{u}},\delta\hat{\mathbf{u}})}(\Delta\hat{\mathbf{u}}) = \frac{1}{2}\left(\delta\hat{\mathbf{u}}_{,\alpha}\cdot\Delta\hat{\mathbf{u}}_{,\beta} + \Delta\hat{\mathbf{u}}_{,\alpha}\cdot\delta\hat{\mathbf{u}}_{,\beta}\right)\hat{\mathbf{G}}^{\alpha}\otimes\hat{\mathbf{G}}^{\beta}. \tag{82}$$

In order to state the expression for the derivative of the variation of the change of curvature tensor we consider the derivative of the Christoffel symbols for the current configuration first. With (77), we have

$$\begin{aligned}\Delta\hat{\Gamma}^{\gamma}_{\alpha\beta} &= \Delta\hat{\mathbf{g}}^{\gamma}\cdot\hat{\mathbf{g}}_{\alpha,\beta} + \hat{\mathbf{g}}^{\gamma}\cdot\Delta\hat{\mathbf{g}}_{\alpha,\beta}\\ &= \hat{\mathbf{g}}_{\alpha,\beta}\cdot(g^{\gamma\varphi}\hat{\mathbf{v}}\otimes\hat{\mathbf{v}} - \hat{\mathbf{g}}^{\varphi}\otimes\hat{\mathbf{g}}^{\gamma})\cdot\Delta\hat{\mathbf{u}}_{,\varphi} + \hat{\mathbf{g}}^{\gamma}\cdot\Delta\hat{\mathbf{u}}_{,\alpha\beta}\\ &= \left(h_{\alpha\beta}g^{\gamma\varphi}\hat{\mathbf{v}} - \Gamma^{\varphi}_{\alpha\beta}\hat{\mathbf{g}}^{\gamma}\right)\cdot\Delta\hat{\mathbf{u}}_{,\varphi} + \hat{\mathbf{g}}^{\gamma}\cdot\Delta\hat{\mathbf{u}}_{,\alpha\beta}.\end{aligned} \tag{83}$$

Thus, the derivative of the variation of the change of curvature tensor is given by (see also [14])

$$\begin{aligned}\Delta\hat{\mathcal{K}}_{(\hat{\mathbf{u}},\delta\hat{\mathbf{u}})}(\Delta\hat{\mathbf{u}}) &= \left[\Delta\hat{\mathbf{v}}\cdot(\delta\hat{\mathbf{u}}_{,\alpha\beta} - \Gamma^{\gamma}_{\alpha\beta}\delta\hat{\mathbf{u}}_{,\gamma}) - \Delta\Gamma^{\gamma}_{\alpha\beta}(\hat{\mathbf{v}}\cdot\delta\hat{\mathbf{u}}_{,\gamma})\right]\hat{\mathbf{G}}^{\alpha}\otimes\hat{\mathbf{G}}^{\beta}\\ &= \Big[(\hat{\mathbf{v}}\cdot\Delta\hat{\mathbf{u}}_{,\varphi})\hat{\mathbf{g}}^{\varphi}\cdot(\delta\hat{\mathbf{u}}_{,\alpha\beta} - \Gamma^{\gamma}_{\alpha\beta}\delta\hat{\mathbf{u}}_{,\gamma}) + \left(\Delta\hat{\mathbf{u}}_{,\alpha\beta} - \Gamma^{\varphi}_{\alpha\beta}\Delta\hat{\mathbf{u}}_{,\varphi}\right)\cdot\hat{\mathbf{g}}^{\gamma}(\hat{\mathbf{v}}\cdot\delta\hat{\mathbf{u}}_{,\gamma})\\ &\quad + \hat{h}_{\alpha\beta}\hat{g}^{\gamma\varphi}(\hat{\mathbf{v}}\cdot\Delta\hat{\mathbf{u}}_{,\varphi})(\hat{\mathbf{v}}\cdot\delta\hat{\mathbf{u}}_{,\gamma})\Big]\hat{\mathbf{G}}^{\alpha}\otimes\hat{\mathbf{G}}^{\beta}.\end{aligned} \tag{84}$$

The linearization of the external virtual work reads

$$LR^{ext}_{(\hat{\mathbf{u}},\delta\hat{\mathbf{u}})}(\Delta\hat{\mathbf{u}}) = R_{ext}(\hat{\mathbf{u}},\delta\hat{\mathbf{u}}) + \Delta R^{ext}_{(\hat{\mathbf{u}},\delta\hat{\mathbf{u}})}(\Delta\hat{\mathbf{u}}) \tag{85}$$

with

$$\Delta R^{ext}_{(\hat{\mathbf{u}},\delta\hat{\mathbf{u}})}(\Delta\hat{\mathbf{u}}) = \int_{\partial U_m}(\Delta\delta\hat{\mathbf{v}}\times\hat{\mathbf{v}} + \delta\hat{\mathbf{v}}\times\Delta\hat{\mathbf{v}})\cdot\hat{\mathbf{T}}^{*}_{m}\hat{J}_b\,\mathrm{d}s_{\theta} \tag{86}$$

The derivative of the variation of the normal vector is

$$\begin{aligned}\Delta\delta\hat{\mathbf{v}}_{(\hat{\mathbf{u}},\delta\hat{\mathbf{u}})}(\Delta\hat{\mathbf{u}}) = \hat{\mathbf{g}}^{\alpha}\left[(\Delta\hat{\mathbf{u}}_{,\alpha}\cdot\hat{\mathbf{g}}^{\beta})(\delta\hat{\mathbf{u}}_{,\beta}\cdot\hat{\mathbf{v}}) + (\delta\hat{\mathbf{u}}_{,\alpha}\cdot\hat{\mathbf{g}}^{\beta})(\Delta\hat{\mathbf{u}}_{,\beta}\cdot\hat{\mathbf{v}})\right]\\ - \hat{\mathbf{v}}\left[\hat{g}^{\alpha\beta}(\delta\hat{\mathbf{u}}_{,\alpha}\cdot\hat{\mathbf{v}})(\Delta\hat{\mathbf{u}}_{,\beta}\cdot\hat{\mathbf{v}})\right],\end{aligned} \tag{87}$$

because taking the derivative of (A.25) results in

$$\begin{aligned}\hat{\mathbf{g}}_{\alpha}\cdot\Delta\delta\hat{\mathbf{v}} &= -\Delta\hat{\mathbf{g}}_{\alpha}\cdot\delta\hat{\mathbf{v}} - \Delta\delta\hat{\mathbf{g}}_{\alpha}\cdot\hat{\mathbf{v}} - \delta\hat{\mathbf{g}}_{\alpha}\cdot\Delta\hat{\mathbf{v}}\\ &= (\Delta\hat{\mathbf{u}}_{,\alpha}\cdot\hat{\mathbf{g}}^{\beta})(\delta\hat{\mathbf{u}}_{,\beta}\cdot\hat{\mathbf{v}}) + (\delta\hat{\mathbf{u}}_{,\alpha}\cdot\hat{\mathbf{g}}^{\beta})(\Delta\hat{\mathbf{u}}_{,\beta}\cdot\hat{\mathbf{v}}),\\ \hat{\mathbf{v}}\cdot\Delta\delta\hat{\mathbf{v}} &= -\Delta\hat{\mathbf{v}}\cdot\delta\hat{\mathbf{v}} = -\hat{g}^{\alpha\beta}(\delta\hat{\mathbf{u}}_{,\alpha}\cdot\hat{\mathbf{v}})(\Delta\hat{\mathbf{u}}_{,\beta}\cdot\hat{\mathbf{v}}).\end{aligned}$$

## 5. Code verification based on an implicit surface description

The isogeometric discretization of (71) and (72) has been implemented in an in-house Matlab code. For the sake of code verification by manufactured solutions, we consider the case of an implicit surface description by the level-set function $\phi : \mathbb{R}^3 \to \mathbb{R}$ such that $\Omega = \{\mathbf{X}\in\mathbb{R}^3 \mid \phi(\mathbf{X}) = 0\}$. Therefore, the code verification for linear shells in [12] is extended to the non-linear case. We refer to [10,11,62] for manufactured solutions based on parametric surface descriptions and linear shell analysis.

As IGA is based on an parametric domain description, the choice of an implicit description seems not natural. However, the present approach has two advantages over a parametric surface description. First, the equations for obtaining the manufactured solution and the equations of the implemented method are different and independent from each other. Thus, both sets of equations have to be correctly implemented, which makes the verification more rigor. The second advantage is that the resulting terms are simpler and numerically stable to evaluate (see [11] for numerical issues).

As inputs for the manufactured solution we need a level-set function $\phi(\mathbf{X})$ describing the problem geometry and a displacement field $\mathbf{u}(\mathbf{X})$. For given $\phi(\mathbf{X})$ we can compute the surface geometry by

$$\boldsymbol{\nu}_0(\mathbf{X}) = \frac{\nabla\phi(\mathbf{X})}{|\nabla\phi(\mathbf{X})|}, \tag{88a}$$

$$\mathbf{P}(\mathbf{X}) = \mathbf{I} - \boldsymbol{\nu}_0(\mathbf{X}) \otimes \boldsymbol{\nu}_0(\mathbf{X}), \tag{88b}$$

$$\mathbf{H}(\mathbf{X}) = -\nabla_\Omega \boldsymbol{\nu}_0(\mathbf{X}). \tag{88c}$$

Once a displacement field $\mathbf{u}(\mathbf{X})$ is chosen as a function of the global coordinates $\mathbf{X}$, the necessary body force for equilibrium can be obtained by the equations given in Section 3, which are summarized here for convenience:

$$\boldsymbol{\varphi}(\mathbf{X}) = \mathbf{X} + \mathbf{u}(\mathbf{X}), \tag{89a}$$

$$\mathbf{F}(\mathbf{X}) = \nabla_\Omega \boldsymbol{\varphi}(\mathbf{X}), \tag{89b}$$

$$J(\mathbf{X}) = |\operatorname{cof} \mathbf{F}(\mathbf{X}) \cdot \boldsymbol{\nu}_0(\mathbf{X})|, \tag{89c}$$

$$\bar{\boldsymbol{\nu}}(\mathbf{X}) = \frac{\operatorname{cof} \mathbf{F}(\mathbf{X}) \cdot \boldsymbol{\nu}_0(\mathbf{X})}{J(\mathbf{X})}, \tag{89d}$$

$$\bar{\mathbf{h}}(\mathbf{X}) = -\nabla_\Omega \bar{\boldsymbol{\nu}}(\mathbf{X}), \tag{89e}$$

$$\mathbf{E}(\mathbf{X}) = \frac{1}{2}(\mathbf{F}^\top(\mathbf{X}) \cdot \mathbf{F}(\mathbf{X}) - \mathbf{P}(\mathbf{X})), \tag{89f}$$

$$\mathbf{K}(\mathbf{X}) = \mathbf{F}^\top(\mathbf{X}) \cdot \bar{\mathbf{h}}(\mathbf{X}) - \mathbf{H}(\mathbf{X}), \tag{89g}$$

$${}^{II}\bar{\mathbf{N}}(\mathbf{X}) = t\left(\bar{\lambda}\mathbf{P}(\mathbf{X}) \operatorname{tr} \mathbf{E}(\mathbf{X}) + 2\mu\mathbf{E}(\mathbf{X})\right), \tag{89h}$$

$${}^{II}\mathbf{M}(\mathbf{X}) = -\frac{t^3}{12}(\bar{\lambda}\,\mathbf{P}(\mathbf{X}) \operatorname{tr} \mathbf{K}(\mathbf{X}) + 2\mu\,\mathbf{K}(\mathbf{X})), \tag{89i}$$

$${}^{I}\mathbf{M}(\mathbf{X}) = \mathbf{F}(\mathbf{X}) \cdot {}^{II}\mathbf{M}(\mathbf{X}), \tag{89j}$$

$${}^{I}\mathbf{N}(\mathbf{X}) = \mathbf{F}(\mathbf{X}) \cdot {}^{II}\bar{\mathbf{N}}(\mathbf{X}) - \bar{\mathbf{h}}(\mathbf{X}) \cdot {}^{II}\mathbf{M}(\mathbf{X}) + \bar{\boldsymbol{\nu}}(\mathbf{X}) \otimes (\mathbf{F}^\dagger(\mathbf{X}) \cdot \operatorname{div}_\Omega {}^{I}\mathbf{M}(\mathbf{X})), \tag{89k}$$

$$\mathbf{B}(\mathbf{X}) = -\operatorname{div}_\Omega {}^{I}\mathbf{N}(\mathbf{X}). \tag{89l}$$

## 6. Numerical results

In this section, we apply manufactured solutions obtained from the procedure in Section 5 to verify the implementation of the isogeometric shell analysis described in Section 4. We have successfully run the method on various geometries, displacement fields and boundary condition combinations. Here, we show the results of 5 examples with increasing complexity, which are described in the following. In principle, it would be sufficient to consider only the most general case in order to verify the implementation, since the special cases are included in the general case. However, in order to have confirmation exercises, we suggest special cases where parts of the code can be tested. In order to allow a reproduction of the tests, the corresponding Matlab files for the geometries, solution fields, stress fields and forcing functions are provided online.[1]

In all examples we used the parameters $E = 4.32 \cdot 10^8$, $\nu = 0.4$, and $t = 0.025$ and the parametric plane $U = [0,1]^2$. In each example, the type of boundary condition (Dirichlet or Neumann) are chosen arbitrarily for each of the four edges. The prescribed values of $\mathbf{u}$ and $\mathbf{T}_\sigma$ are taken from the manufactured solution.

In the following, we study the convergence of the absolute $L_2$-error in the displacements

$$e_u = \|\mathbf{u} - \mathbf{u}^{ex}\|_{L_2} = \sqrt{\int_\Omega (\mathbf{u} - \mathbf{u}^{ex}) \cdot (\mathbf{u} - \mathbf{u}^{ex})\, d\mathbf{X}}, \tag{90}$$

where $\mathbf{u}^{ex}$ is the chosen displacement field and $\mathbf{u}$ the numerically computed displacement solution.

### 6.1. Flat geometry

We begin our presentation with two examples on initially flat geometries, which are described by the level-set function $\phi(x, y, z) = z$. In the first example, we use as initial configuration the unit square. Therefore, no geometry mapping between parameter plane

[1] https://github.com/michaelgfrerer/nonlinear-shell-verification

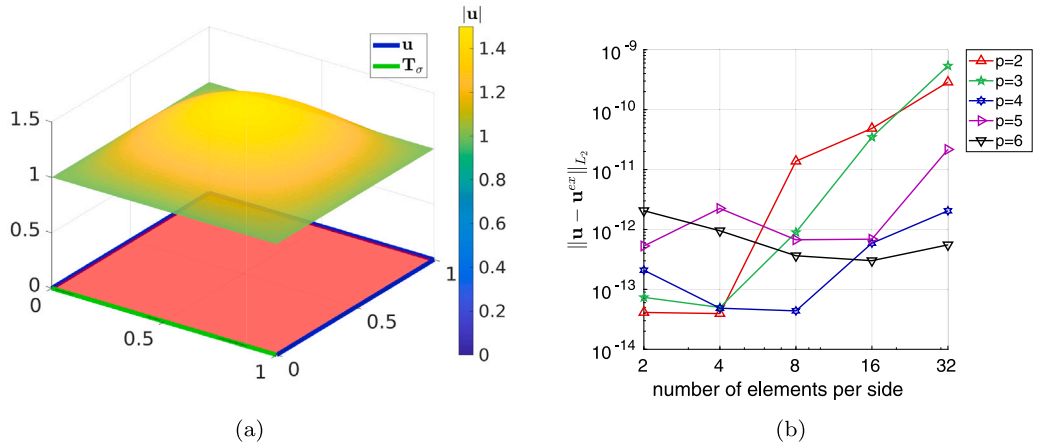


**Fig. 1.** Verification example 1: (a) The initial (red surface) and the deformed configurations are shown. The prescribed boundary conditions are indicated on the edges of the initial configuration. The magnitude of the displacement field is plotted over the deformed geometry. (b) The convergence results for the $L_2$-error together their theoretical counterparts (dashed lines) are shown.

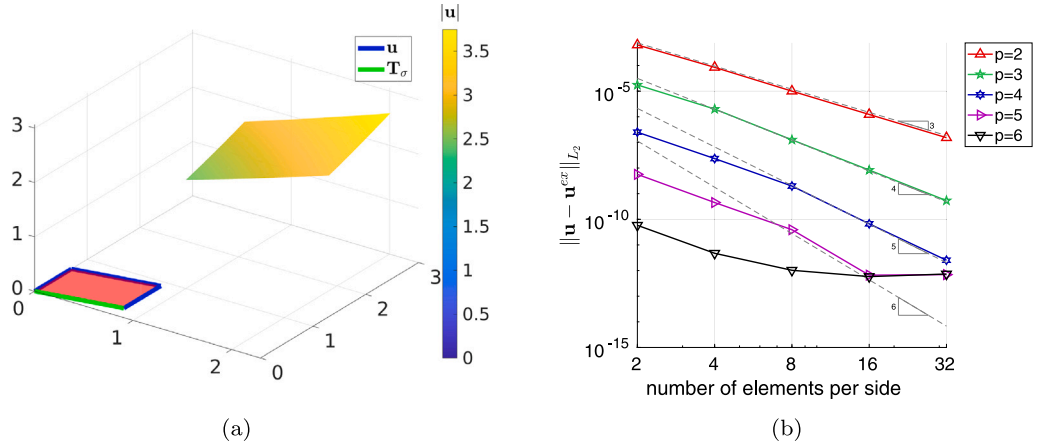


**Fig. 2.** Verification example 2: (a) The initial (red surface) and the deformed configurations are shown. The prescribed boundary conditions are indicated on the edges of the initial configuration. The magnitude of the displacement field is plotted over the deformed geometry. (b) The convergence results for the L 2 -error together their theoretical counterparts (dashed lines) are shown.

and initial geometry is involved and thus, the numerical integration does not add an error due to integral approximation. For the displacement field we have chosen (see Fig. 1(a))

$$\mathbf{u}_1(x,y,z) = (1 + 8xy\,(x-1)\,(y-1))\,\mathbf{e}_3, \tag{91}$$

which is a bi-variate polynomial of order two and thus, can be exactly represented in the ansatz space. Therefore, the numerically computed displacement field is exact up to round-of errors. This can be seen from the numerical results of the displacement error $e_u$ illustrated in Fig. 1(b). In the second example, we use a distorted square as initial geometry, which is described by the parametrization

$$\mathfrak{G}_2(\theta_1,\theta_2) = \frac{4\theta_1}{5}\mathbf{e}_1 + \left(\frac{\theta_1}{5} + \frac{7\theta_2}{10}\right)\mathbf{e}_2. \tag{92}$$

For the numerical simulation this geometry is represented by NURBS/B-splines. The chosen displacement field is given by

$$\mathbf{u}_2(x,y,z) = \mathrm{e}^{\frac{x}{2}}\mathbf{e}_1 + \mathrm{e}^{\frac{y}{2}}\mathbf{e}_2 + \left(\mathrm{e}^{\frac{x}{2}} + \mathrm{e}^{\frac{y}{2}}\right)\mathbf{e}_3. \tag{93}$$

The initial and deformed configurations and the numerical results for (92) and (93) are depicted in Fig. 2. For the error $e_u$ we observe optimal $p+1$ convergence up to an error level of $10^{12}$.

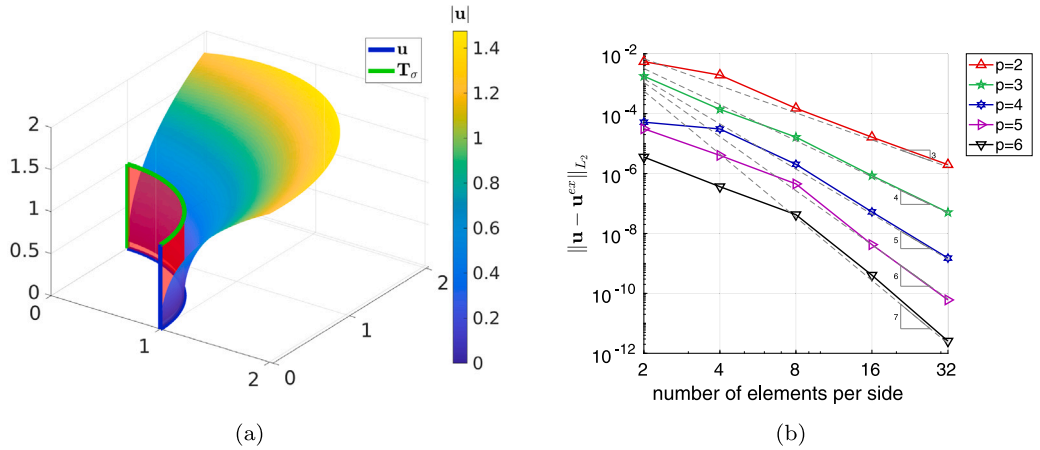


**Fig. 3.** Verification example 3: (a) The initial (red surface) and the deformed configurations are shown. The prescribed boundary conditions are indicated on the edges of the initial configuration. The magnitude of the displacement field is plotted over the deformed geometry. (b) The convergence results for the L 2 -error together their theoretical counterparts (dashed lines) are shown.

### 6.2. Parabolic geometry

In example 3, we consider a cylindrical shell and therefore, a parabolic geometry with constant mean curvature. For the manufactured solution the geometry is described by the level-set function $\phi(x,y,z) = x^2 + y^2 - 1$. In the verification test we use one quarter of a cylinder with radius $r = 1$ and height $h = 1$ as initial geometry. The chosen displacement field as a function of $(x,y,z)$ is given by

$$\mathbf{u}_3(x,y,z) = xz^2\mathbf{e}_1 + yz^2\mathbf{e}_2 + \tanh(z)\mathbf{e}_3. \tag{94}$$

We remark that for this example the resulting forcing function, as well as the stress field, are drastically more complex than for the previous examples (see also Table 1). The initial and the deformed configurations and the numerical results of the convergence study are illustrated in Fig. 3. For the error $e_u$ we observe optimal $p+1$ convergence.

### 6.3. Elliptic geometry

In verification example 4, we consider a part of a spherical shell and therefore, an elliptic geometry with constant non-vanishing Gaussian curvature. For the manufactured solution, we describe the geometry by the level-set function

$$\phi(x,y,z) = x^2 + y^2 + z^2 - 1, \tag{95}$$

whereas in the verification test of the numerical method the initial surface is obtained by revolving a circular arc (central angle of $\frac{180}{\pi}^\circ$ and unit radius) by an angle of $\frac{180}{\pi}^\circ$. The chosen displacement field over the spherical shell as a function of $(x,y,z)$ is given by

$$\mathbf{u}_4(x,y,z) = x^2\mathbf{e}_1 + y^2\mathbf{e}_2 + z^2\mathbf{e}_3. \tag{96}$$

Again, for this example the resulting forcing function and the stress field is highly complex (see Table 1).

The initial an the deformed configurations and the numerical results are illustrated in Fig. 4. For the error $e_u$, we observe optimal $p+1$ convergence.

### 6.4. Geometry with varying curvature

In the last example, we consider a geometry where the curvature changes over the shell surface. For the manufactured solution the level-set function is

$$\phi(x,y,z) = z - xy. \tag{97}$$

For the simulation we use a NURBS/B-spline representation of the surface described by the parametrization

$$\mathfrak{G}_5(\theta_1,\theta_2) = \theta_1\mathbf{e}_1 + \theta_2\mathbf{e}_2 + \theta_1\theta_2\mathbf{e}_3, \tag{98}$$

The chosen displacement for example 5 as a function of $(x,y,z)$ is given by

$$\mathbf{u}_5(x,y,z) = \mathrm{e}^z\mathbf{e}_3, \tag{99}$$

The initial and the deformed configurations are visualized in Fig. 5(a). The numerical results of the convergence study are plotted in Fig. 5(b). For the $L_2$-error we observe optimal $p+1$ convergence.

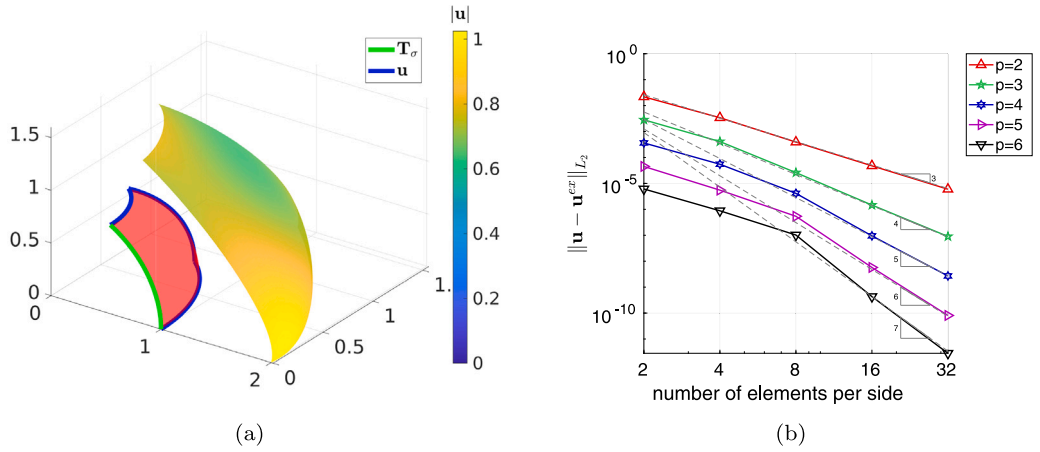


**Fig. 4.** Verification example 4: (a) The initial (red surface) and the deformed configurations are shown. The prescribed boundary conditions are indicated on the edges of the initial configuration. The magnitude of the displacement field is plotted over the deformed geometry. (b) The convergence results for the $L_2$-error together their theoretical counterparts (dashed lines) are shown.

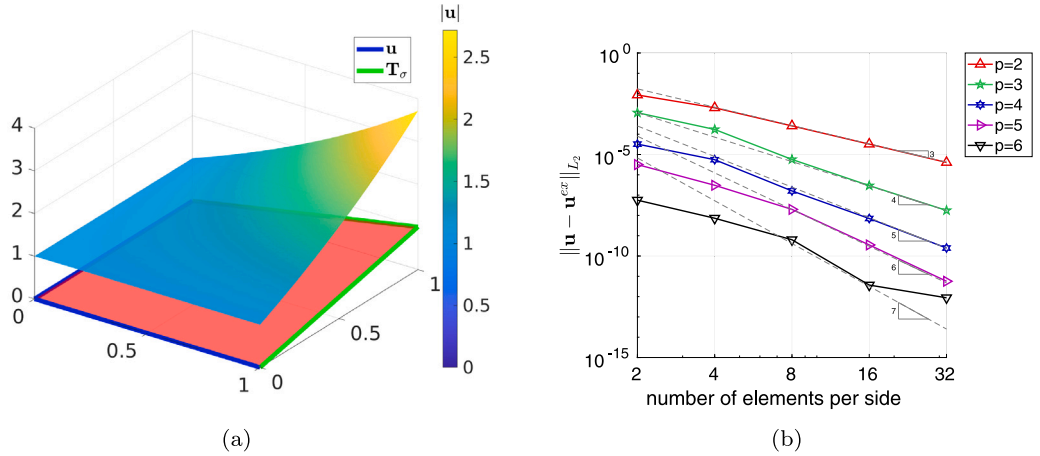


**Fig. 5.** Verification example 5: (a) The initial (red surface) and the deformed configurations are shown. The prescribed boundary conditions are indicated on the edges of the initial configuration. The magnitude of the displacement field is plotted over the deformed geometry. (b) The convergence results for the L 2 -error together their theoretical counterparts (dashed lines) are shown.

### *6.5. Comparison with manufactured solutions based on parametric surface descriptions*

In this section we compare the proposed methodology in Section 5 against manufactured solutions based on parametrizations (see [10,11] for linear Kirchhoff–Love shells). To this end, we also implemented the strong form of the non-linear Kirchhoff–Love shells for parametrized surfaces (see e.g. [14]) using symbolic calculations in Matlab. All computations are performed on a personal computer with an AMD Ryzen 7 3700X 8-Core processor with 64 GB RAM, which uses an Ubuntu 22.04 operating system. The computation times for the generation of the manufactured solutions are summarized in Table 1. In most of the examples the computation time for the "implicit manufactured solution" was significantly lower than for the respective "parametric manufactured solution". Moreover, due to memory restrictions we were not able to obtain a "parametric manufactured solution" for examples 3 and 4.

## 7. Conclusion

We have performed rigorous code verification based on manufactured solutions for geometrically non-linear Kirchhoff–Love shells for the first time. As a numerical method we used IGA. Thus, the governing equations for the discretization method are based on a parametrization of the shell surface. In order to decouple the IGA and the manufactured solution we used a implicit surface description for the latter. Due to this decoupling the obtained manufactured solutions can be readily used also for the verification of other discretization methods. When a parametrization is used the sought displacement field and the corresponding forcing functions

**Table 1**
Computation times to generate the manufactured solutions used in Sections 6.1–6.4. The column "implicit" uses the methodology introduced in Section 5, whereas the column "parametric" refers to a methodology, where the sought displacement field is defined over the parameter domain.

| | implicit | parametric |
|---|---|---|
| Example 1 | ~30 s | ~196 s |
| Example 2 | ~298 s | ~1520 s |
| Example 3 | ~14000 s | n.a. |
| Example 4 | ~11451 s | n.a. |
| Example 5 | ~2350 s | ~875 s |

are functions defined on the parameter plane. In contrast to this, when a implicit surface description is used, the displacement field is chosen as a function on $\mathbb{R}^3$. In order to obtain the corresponding forcing function also in this setting we used TDC to derive the parametrization-free governing equations of non-linear Kirchhoff–Love shells in strong form.

In future work, several research directions seem to be of interest. Firstly, other shell models, e.g. non-linear Reissner–Mindlin (5-parameter) or three-dimensional (7-parameter) shells, could be formulated in a coordinate-free way, enabling manufactured solutions based on implicit surface descriptions. Secondly, the manufactured solutions could be applied to IGA multi-patch analysis and other discretization methods. Due to the implicit surface descriptions, this should be easily possible. Thirdly, the extension to non-linear constitutive equations would be possible. Lastly, the presented formulation of the governing equations by means of TDC would allow the development of unfitted finite element methods like the TraceFEM and the CutFEM for non-linear Kirchhoff–Love shells.

## Declaration of competing interest

The authors declare that they have no known competing financial interests or personal relationships that could have appeared to influence the work reported in this paper.

## Data availability

In order to allow a reproduction of the tests, the corresponding Matlab files are provided online at https://github.com/michael-gfrerer/nonlinear-shell-verification

## Acknowledgments

This research did not receive any specific grant from funding agencies in the public, commercial, or not-for-profit sectors.

## Appendix. Proofs

### A.1. Proof of Lemma 3.2

In order to show (35) we first show the relation

$$\operatorname{div}_\Omega(J(\mathbf{X})\mathbf{F}^\dagger(\mathbf{X})^\top) = J(\mathbf{X})\, h(\boldsymbol{\varphi}(\mathbf{X}))\boldsymbol{\nu}(\boldsymbol{\varphi}(\mathbf{X})). \tag{A.1}$$

To this end we use local coordinates. We note the relations

$$J\circ g(\theta) = \frac{|\hat{\mathbf{g}}_1\times\hat{\mathbf{g}}_2|}{|\hat{\mathbf{g}}_1\times\hat{\mathbf{G}}_2|}, \tag{A.2a}$$

$$(J\circ g(\theta))_{,\beta} = J\,\Gamma^\alpha_{\alpha\beta} - \frac{J\,\hat{\Gamma}^\alpha_{\alpha\beta}}{|\hat{\mathbf{G}}_1\times\hat{\mathbf{G}}_2|^2}, \tag{A.2b}$$

$$\hat{\mathbf{g}}^\beta_{,\beta} = -\Gamma^\beta_{\beta\alpha}\hat{\mathbf{g}}^\alpha + \hat{h}\hat{\boldsymbol{\nu}}, \tag{A.2c}$$

$$\hat{\mathbf{G}}_{\alpha,\beta}\cdot\hat{\mathbf{G}}^\beta = \hat{\Gamma}^\beta_{\alpha\beta}. \tag{A.2d}$$

Therefore, we have

$$\begin{aligned}\mathrm{div}_\Omega(J(\mathbf{X})\mathbf{F}^\dagger(\mathbf{X})^\top)\circ g(\theta) &= \left(\frac{|\hat{\mathbf{g}}_1\times\hat{\mathbf{g}}_2|}{|\hat{\mathbf{G}}_1\times\hat{\mathbf{G}}_2|}\left(\hat{\mathbf{g}}^\alpha\otimes\hat{\mathbf{G}}_\alpha\right)\right)_{,\beta}\cdot\hat{\mathbf{G}}^\beta\\ &= \frac{|\hat{\mathbf{g}}_1\times\hat{\mathbf{g}}_2|}{|\hat{\mathbf{G}}_1\times\hat{\mathbf{G}}_2|}\left(\Gamma^\alpha_{\alpha\beta}-\frac{\hat{\Gamma}^\alpha_{\alpha\beta}}{|\hat{\mathbf{G}}_1\times\hat{\mathbf{G}}_2|^2}\right)\hat{\mathbf{g}}^\beta\\ &+\left(\frac{|\hat{\mathbf{g}}_1\times\hat{\mathbf{g}}_2|}{|\hat{\mathbf{G}}_1\times\hat{\mathbf{G}}_2|}\right)\left(\hat{\mathbf{g}}^\beta_{,\beta}+\hat{\mathbf{g}}^\alpha(\hat{\mathbf{G}}_{\alpha,\beta}\cdot\hat{\mathbf{G}}^\beta)\right)\\ &= \frac{|\hat{\mathbf{g}}_1\times\hat{\mathbf{g}}_2|}{|\hat{\mathbf{G}}_1\times\hat{\mathbf{G}}_2|}\hat{h}\,\hat{\mathbf{v}},\end{aligned} \tag{A.3}$$

and relation (A.1) follows. Thus, with (A.1) and

$$\begin{aligned}(\nabla_{\mathbf{X}}\boldsymbol{\sigma}(\boldsymbol{\varphi}(\mathbf{X}))\cdot\mathbf{P}_0(\mathbf{X}))\,:\,\mathbf{F}^\dagger(\mathbf{X}) &= (\nabla_{\mathbf{x}}\boldsymbol{\sigma}(\mathbf{x})\cdot\mathbf{F}(\mathbf{X})\cdot\mathbf{P}_0(\mathbf{X}))\,:\,\mathbf{F}^\dagger(\mathbf{X})\circ\boldsymbol{\varphi}(\mathbf{X})\\ &= \nabla_{\mathbf{x}}\boldsymbol{\sigma}(\mathbf{x})\,:\,(\mathbf{F}(\mathbf{X})\cdot\mathbf{F}^\dagger(\mathbf{X}))\circ\boldsymbol{\varphi}(\mathbf{X})\\ &= (\nabla_{\mathbf{x}}\boldsymbol{\sigma}(\mathbf{x})\,:\,\mathbf{P}_t(\mathbf{X}))\circ\boldsymbol{\varphi}(\mathbf{X}),\end{aligned} \tag{A.4}$$

we have

$$\begin{aligned}\mathrm{div}_\Omega{}^I\mathbf{N}(\mathbf{X}) &= \nabla_\Omega\boldsymbol{\sigma}(\mathbf{x}(\mathbf{X}))\,:\,(J(\mathbf{X})(\mathbf{F}^\dagger)) + \boldsymbol{\sigma}(\boldsymbol{\varphi}(\mathbf{X}))\cdot\mathrm{div}_\Omega(J(\mathbf{X})(\mathbf{F}^\dagger)^\top)\\ &= J(\mathbf{X})\left((\nabla_{\mathbf{X}}\boldsymbol{\sigma}(\boldsymbol{\varphi}(\mathbf{X}))\cdot\mathbf{P}_0)\,:\,\mathbf{F}^\dagger + J(\mathbf{X})h(\boldsymbol{\varphi}(\mathbf{X}))\boldsymbol{\sigma}(\boldsymbol{\varphi}(\mathbf{X}))\cdot\boldsymbol{\nu}(\boldsymbol{\varphi}(\mathbf{X}))\right)\\ &= J(\mathbf{X})\mathrm{div}_\omega(\boldsymbol{\sigma}(\mathbf{x}))\circ\boldsymbol{\varphi}(\mathbf{X}).\end{aligned} \tag{A.5}$$

In order to derive the local force equilibrium in the initial configuration we transform (32) to the initial configuration

$$\int_\Omega(\mathrm{div}_\omega\,\boldsymbol{\sigma}(\mathbf{x})+\mathbf{b}(\mathbf{x}))\circ\boldsymbol{\varphi}(\mathbf{X})\;J(\mathbf{X})\;\mathrm{d}\mathbf{X}=\mathbf{0}. \tag{A.6}$$

With (35) we have

$$\int_\Omega \mathrm{div}_\Omega{}^I\mathbf{N}(\mathbf{X})+\mathbf{B}(\mathbf{X})\;\mathrm{d}\mathbf{X}=\mathbf{0} \tag{A.7}$$

from which (36) follows by localization.

### A.2. Proof of Lemma 3.6

We multiply the strong form (33) by the velocity and integrate over the current shell surface,

$$\int_\omega \mathbf{v}\cdot(\mathrm{div}\;\boldsymbol{\sigma}+\mathbf{b})\;\mathrm{d}\mathbf{x}=0 \tag{A.8}$$

Applying integration by parts (12) results in

$$\int_\omega\nabla_\omega\mathbf{v}\,:\,\boldsymbol{\sigma}^\top\;\mathrm{d}\mathbf{x}=\int_\gamma\mathbf{v}\cdot\boldsymbol{\sigma}\cdot\boldsymbol{\mu}\;\mathrm{d}s_{\mathbf{x}}+\int_\omega\mathbf{v}\cdot\mathbf{b}\;\mathrm{d}\mathbf{x}. \tag{A.9}$$

For the integral on the left side we further get

$$\begin{aligned}\int_\omega\nabla_\omega\mathbf{v}\,:\,\boldsymbol{\sigma}^\top\;\mathrm{d}\mathbf{x} &= \int_\omega\nabla_\omega\mathbf{v}\,:\,(\bar{\mathbf{n}}-\mathbf{m}\cdot\mathbf{h}+\mathbf{P}_t\cdot\mathrm{div}\;\mathbf{m}\otimes\boldsymbol{\nu})\;\mathrm{d}\mathbf{x}\\ &= \int_\omega\nabla_\omega\mathbf{v}\,:\,\bar{\mathbf{n}}-(\mathbf{h}\cdot\nabla_\omega\mathbf{v})\,:\,\mathbf{m}+(\boldsymbol{\nu}\cdot\nabla_\omega\mathbf{v})\cdot\mathrm{div}\;\mathbf{m}\;\mathrm{d}\mathbf{x}.\end{aligned} \tag{A.10}$$

Applying integration by parts (12) to the last term on the right side yields

$$\int_\omega(\boldsymbol{\nu}\cdot\nabla_\omega\mathbf{v})\cdot\mathrm{div}\;\mathbf{m}\;\mathrm{d}\mathbf{x}=-\int_\omega\nabla_\omega(\boldsymbol{\nu}\cdot\nabla_\omega\mathbf{v})\,:\,\mathbf{m}\;\mathrm{d}\mathbf{x}+\int_\gamma(\boldsymbol{\nu}\cdot\nabla_\omega\mathbf{v})\cdot\mathbf{m}\cdot\boldsymbol{\mu}\;\mathrm{d}s_{\mathbf{x}}. \tag{A.11}$$

Due to

$$(\mathbf{h}\cdot\nabla_\omega\mathbf{v}+\nabla_\omega(\boldsymbol{\nu}\cdot\nabla_\omega\mathbf{v}))\,:\,\mathbf{m}=(\boldsymbol{\nu}\cdot\nabla_\omega\nabla_\omega\mathbf{v})\,:\,\mathbf{m}, \tag{A.12}$$

where we used that $\mathbf{m}$ is tangential, and $\bar{\mathbf{n}}$ being tangential and symmetric, we obtain (46). Next we show (49). Recalling (21) we have

$$\nabla_\omega\mathbf{v}(\mathbf{x})\circ\boldsymbol{\varphi}(\mathbf{X})=\nabla_\Omega\mathbf{v}(\boldsymbol{\varphi}(\mathbf{X}))\cdot\mathbf{F}^\dagger=\dot{\mathbf{F}}\cdot\mathbf{F}^\dagger, \tag{A.13}$$

due to $\dot{\mathbf{F}}=\nabla_\Omega\mathbf{V}$. Furthermore, we note that

$$\dot{\mathbf{E}}=\frac{1}{2}(\dot{\mathbf{F}}^T\cdot\mathbf{F}+\mathbf{F}^T\cdot\dot{\mathbf{F}}) \tag{A.14}$$

because of the product rule, and obtain

$$\begin{aligned}\mathbf{d}(\mathbf{x})\circ\boldsymbol{\varphi}(\mathbf{X}) &= \frac{1}{2}(\mathbf{F}^{\dagger\top}\cdot\mathbf{F}^{\top})\cdot(\dot{\mathbf{F}}\cdot\mathbf{F}^{\dagger}+\mathbf{F}^{\dagger\top}\cdot\dot{\mathbf{F}}^{\top})\cdot(\mathbf{F}\cdot\mathbf{F}^{\dagger})\\ &= \frac{1}{2}\mathbf{F}^{\dagger\top}\cdot(\mathbf{F}^{\top}\cdot\dot{\mathbf{F}}+\dot{\mathbf{F}}^{\top}\cdot\mathbf{F})\cdot\mathbf{F}^{\dagger}\\ &= \mathbf{F}^{\dagger\top}\cdot\dot{\mathbf{E}}\cdot\mathbf{F}^{\dagger}\end{aligned} \tag{A.15}$$

Now we consider the membrane part in (46), *i.e.* the first term on the left side, and obtain

$$\begin{aligned}\int_{\omega}\mathbf{d}(\mathbf{x}) : \bar{\mathbf{n}}(\mathbf{x})\,\mathrm{d}\mathbf{x} &= \int_{\Omega}((\mathbf{F}^{\dagger})^{\top}\cdot\dot{\mathbf{E}}\cdot\mathbf{F}^{\dagger}) : \bar{\mathbf{n}}(\mathbf{x}))\circ\varphi(\mathbf{X})J(\mathbf{X})\,\mathrm{d}\mathbf{X}\\ &= \int_{\Omega}\dot{\mathbf{E}} : (\mathbf{F}^{\dagger}\cdot\bar{\mathbf{n}}(\varphi(\mathbf{X}))\cdot(\mathbf{F}^{\dagger})^{\top})J(\mathbf{X})\,\mathrm{d}\mathbf{X}\\ &= \int_{\Omega}\dot{\mathbf{E}}(\mathbf{X}) : {}^{II}\bar{\mathbf{N}}(\mathbf{X})\,\mathrm{d}\mathbf{X},\end{aligned} \tag{A.16}$$

where we used that $\bar{\mathbf{n}}$ is a tangential tensor. In the next step we consider the bending part in (46), *i.e.* the second term on the left side, where we have to show the relation

$$\left[\boldsymbol{\nu}(\mathbf{x})\cdot(\nabla_{\omega}\nabla_{\omega}\mathbf{v}(\mathbf{x})) : \mathbf{m}(\mathbf{x})\right]\circ\boldsymbol{\varphi}(\mathbf{X})J(\mathbf{X}) = \dot{\mathbf{K}}(\mathbf{X}) : {}^{II}\mathbf{M}(\mathbf{X}) \tag{A.17}$$

Using the definition (48) we have

$$\begin{aligned}\dot{\mathbf{K}}(\mathbf{X}) : {}^{II}\mathbf{M}(\mathbf{X}) &= \dot{\mathbf{K}}(\mathbf{X}) : \left[\mathbf{F}^{\dagger}(\mathbf{X})\cdot\mathbf{m}(\varphi(\mathbf{X}))\cdot\mathbf{F}^{\dagger}(\mathbf{X})^{\top}J(\mathbf{X})\right]\\ &= \left[\mathbf{F}^{\dagger}(\mathbf{X})^{\top}\cdot\dot{\mathbf{K}}(\mathbf{X})\cdot\mathbf{F}^{\dagger}(\mathbf{X})\right] : \mathbf{m}(\varphi(\mathbf{X}))J(\mathbf{X}).\end{aligned} \tag{A.18}$$

We now proceed by resorting to local coordinates and note that

$$\begin{aligned}\dot{\mathbf{K}}\circ\mathfrak{g}(\theta) &= (\dot{\hat{\boldsymbol{\nu}}}\cdot\hat{\mathbf{g}}_{\alpha,\beta}+\hat{\boldsymbol{\nu}}\cdot\dot{\hat{\mathbf{g}}}_{\alpha,\beta})\hat{\mathbf{G}}^{\alpha}\otimes\hat{\mathbf{G}}^{\beta}\\ &= (-(\hat{\boldsymbol{\nu}}\cdot\mathbf{v}_{\gamma})\hat{\mathbf{g}}^{\gamma}\cdot\hat{\mathbf{g}}_{\alpha,\beta}+\hat{\boldsymbol{\nu}}\cdot\mathbf{v}_{,\alpha\beta})\hat{\mathbf{G}}^{\alpha}\otimes\hat{\mathbf{G}}^{\beta}\\ &= \hat{\boldsymbol{\nu}}\cdot(\mathbf{v}_{,\alpha\beta}-\Gamma^{\gamma}_{\alpha\beta}\mathbf{v}_{\gamma})\,\hat{\mathbf{G}}^{\alpha}\otimes\hat{\mathbf{G}}^{\beta}\end{aligned} \tag{A.19}$$

where we use the result given in Lemma 4.1 by noting the relation between variation and time derivative of the normal vector. Thus, on the one hand we have

$$\left[\mathbf{F}^{\dagger}(\mathbf{X})^{\top}\cdot\dot{\mathbf{K}}(\mathbf{X})\cdot\mathbf{F}^{\dagger}(\mathbf{X})\right]\circ\mathfrak{g}(\theta) = \hat{\boldsymbol{\nu}}\cdot(\mathbf{v}_{,\alpha\beta}-\Gamma^{\gamma}_{\alpha\beta}\mathbf{v}_{,\gamma})\,\hat{\mathbf{g}}^{\alpha}\otimes\hat{\mathbf{g}}^{\beta} \tag{A.20}$$

and on the other hand we have

$$\begin{aligned}\left[\boldsymbol{\nu}(\mathbf{x})\cdot(\nabla_{\omega}\nabla_{\omega}\mathbf{v}(\mathbf{x}))\right]\circ\boldsymbol{\varphi}(\mathbf{X})\circ\mathfrak{g}(\theta) &= \hat{\boldsymbol{\nu}}\cdot((\mathbf{v}_{,\alpha}\otimes\hat{\mathbf{g}}^{\alpha})_{,\beta}\otimes\hat{\mathbf{g}}^{\beta})\\ &= \hat{\boldsymbol{\nu}}\cdot\left(\mathbf{v}_{,\alpha\beta}\otimes\hat{\mathbf{g}}^{\alpha}\otimes\hat{\mathbf{g}}^{\beta}+\mathbf{v}_{,\alpha}\otimes\hat{\mathbf{g}}^{\alpha}_{,\beta}\otimes\hat{\mathbf{g}}^{\beta}\right)\\ &= \hat{\boldsymbol{\nu}}\cdot\left(\mathbf{v}_{,\alpha\beta}-\Gamma^{\gamma}_{\alpha\beta}\mathbf{v}_{,\gamma}\right)\hat{\mathbf{g}}^{\alpha}\otimes\hat{\mathbf{g}}^{\beta}+h^{\alpha}_{\beta}(\boldsymbol{\nu}\cdot\mathbf{v}_{,\alpha})\boldsymbol{\nu}\otimes\hat{\mathbf{g}}^{\beta}.\end{aligned} \tag{A.21}$$

Therefore, taking into account that $\mathbf{m}$ is a tangential tensor we have verified (A.17). The surface integral on the right side of (49) immediately follows from the corresponding surface integral in (46) by change of variables. The first boundary integral on the right side of (49) follows from the corresponding surface integral in (46) by Corollary 3.4. For the second boundary integral we observe from Lemma 4.1 that

$$\dot{\bar{\boldsymbol{\nu}}} = -\bar{\boldsymbol{\nu}}\cdot\nabla_{\Omega}\mathbf{V}\cdot\mathbf{F}^{\dagger}, \tag{A.22}$$

and with Corollary 3.4 we have

$$\begin{aligned}\int_{\gamma}\boldsymbol{\nu}\cdot\nabla_{\omega}\mathbf{v}\cdot\mathbf{m}\cdot\boldsymbol{\mu}\,\mathrm{d}s_{\mathbf{x}} &= \int_{\Gamma}(\boldsymbol{\nu}\cdot\nabla_{\omega}\mathbf{v})\circ\boldsymbol{\varphi}(\mathbf{X})\cdot{}^{I}\mathbf{M}\cdot\boldsymbol{\mu}_0\,\mathrm{d}s_{\mathbf{X}}\\ &= \int_{\Gamma}\bar{\boldsymbol{\nu}}\cdot\nabla_{\Omega}\mathbf{V}\cdot\mathbf{F}^{\dagger}\cdot{}^{I}\mathbf{M}\cdot\boldsymbol{\mu}_0\,\mathrm{d}s_{\mathbf{X}}\\ &= -\int_{\Gamma}\dot{\bar{\boldsymbol{\nu}}}\cdot{}^{I}\mathbf{M}\cdot\boldsymbol{\mu}_0\,\mathrm{d}s_{\mathbf{X}}.\end{aligned} \tag{A.23}$$

This finishes the poof of (49).

### *A.3. Proof of Lemma 4.1*

Taking the variation of the identities

$$\begin{aligned}\hat{\mathbf{g}}_{\alpha}\cdot\hat{\boldsymbol{\nu}} &= 0, \qquad & \hat{\boldsymbol{\nu}}\cdot\hat{\boldsymbol{\nu}} &= 1,\\ \hat{\mathbf{g}}_{\alpha}\cdot\hat{\mathbf{g}}^{\beta} &= \delta^{\beta}_{\alpha}, \qquad & \hat{\mathbf{g}}^{\alpha}\cdot\hat{\boldsymbol{\nu}} &= 0,\end{aligned} \tag{A.24}$$

yields by the chain rule

$$\begin{aligned} \hat{\mathbf{g}}_\alpha \cdot \delta\hat{\boldsymbol{\nu}} &= -\delta\hat{\mathbf{g}}_\alpha \cdot \hat{\boldsymbol{\nu}}, \qquad & 2\hat{\boldsymbol{\nu}} \cdot \delta\hat{\boldsymbol{\nu}} &= 0, \\ \hat{\mathbf{g}}_\alpha \cdot \delta\hat{\mathbf{g}}^\beta &= -\delta\hat{\mathbf{g}}_\alpha \cdot \hat{\mathbf{g}}^\beta, \qquad & \delta\hat{\mathbf{g}}^\alpha \cdot \hat{\boldsymbol{\nu}} &= -\hat{\mathbf{g}}^\alpha \cdot \delta\hat{\boldsymbol{\nu}}. \end{aligned} \tag{A.25}$$

It is easily verified that these conditions are fulfilled by (76) and (77).

## References


[1] P. Naghdi, Finite deformation of elastic rods and shells, in: Proceedings of the IUTAM Symposium on Finite Elasticity, Springer, 1981, pp. 47–103.
[2] W. Pietraszkiewicz, Geometrically nonlinear theories of thin elastic shells, Adv. Mech. 12 (1989) 51–130.
[3] M. Bischoff, K.-U. Bletzinger, W. Wall, E. Ramm, Models and finite elements for thin-walled structures, in: E. Stein, R. de Borst, T. Hughes (Eds.), Encyclopedia of Comput Mech, Vol. 2, Wiley Online Library, 2004, pp. 59–137.
[4] J.T. Oden, T. Belytschko, J. Fish, T. Hughes, C. Johnson, D. Keyes, A. Laub, L. Petzold, D. Srolovitz, S. Yip, Revolutionizing engineering science through simulation, Natl. Sci. Found. Blue Ribbon Panel Rep. 65 (2006).
[5] W.L. Oberkampf, C.J. Roy, Verification and Validation in Scientific Computing, Cambridge University Press, 2010.
[6] C.J. Roy, Review of code and solution verification procedures for computational simulation, J. Comput. Phys. 205 (1) (2005) 131–156.
[7] K. Salari, P. Knupp, Code Verification by the Method of Manufactured Solutions, Tech. Rep, Sandia National Lab.(SNL-NM), Albuquerque, NM (United States), 2000.
[8] T. Belytschko, H. Stolarski, W.K. Liu, N. Carpenter, J.S. Ong, Stress projection for membrane and shear locking in shell finite elements, Comput. Methods Appl. Mech. Engrg. 51 (1) (1985) 221–258.
[9] S. Steinberg, P.J. Roache, Symbolic manipulation and computational fluid dynamics, J. Comput. Phys. 57 (2) (1985) 251–284.
[10] M. Gfrerer, M. Schanz, Code verification examples based on the method of manufactured solutions for Kirchhoff–Love and Reissner–Mindlin shell analysis, Eng. Comput. 34 (4) (2018) 775–785.
[11] J. Benzaken, J.A. Evans, S.F. McCormick, R. Tamstorf, Nitsche's method for linear Kirchhoff–Love shells: Formulation, error analysis, and verification, Comput. Methods Appl. Mech. Engrg. 374 (2021) 113544.
[12] M.H. Gfrerer, A $C^1$-continuous Trace-Finite-Cell-Method for linear thin shell analysis on implicitly defined surfaces, Comput. Mech. 67 (2) (2021) 679–697.
[13] Y. Basar, W.B. Krätzig, Mechanik der Flächentragwerke: Theorie, Berechnungsmethoden, Anwendungsbeispiele, Vieweg, 1985.
[14] R.A. Sauer, T.X. Duong, On the theoretical foundations of thin solid and liquid shells, Math. Mech. Solids 22 (3) (2017) 343–371.
[15] E. Burman, S. Claus, P. Hansbo, M. Larson, A. Massing, CutFEM: Discretizing geometry and partial differential equations, Int. J. Numer. Methods Eng. 104 (7) (2015) 472–501.
[16] E. Burman, P. Hansbo, M. Larson, A stabilized cut finite element method for partial differential equations on surfaces: The Laplace–Beltrami operator, Comput. Methods Appl. Mech. Engrg. 285 (2015) 188–207.
[17] E. Burman, P. Hansbo, M.G. Larson, A. Massing, Cut finite element methods for partial differential equations on embedded manifolds of arbitrary codimensions, ESAIM Math. Model. Numer. Anal. 52 (6) (2018) 2247–2282.
[18] M.A. Olshanskii, A. Reusken, Trace finite element methods for PDEs on surfaces, in: S.P.A. Bordas, E. Burman, M.G. Larson, M.A. Olshanskii (Eds.), Geometrically Unfitted Finite Element Methods and Applications, Springer International Publishing, 2017, pp. 211–258.
[19] J. Grande, C. Lehrenfeld, A. Reusken, Analysis of a high-order trace finite element method for PDEs on level set surfaces, SIAM J. Numer. Anal. 56 (1) (2018) 228–255.
[20] M.E. Gurtin, A.I. Murdoch, A continuum theory of elastic material surfaces, Arch. Ration Mech. Anal. 57 (4) (1975) 291–323.
[21] P. Hansbo, M.G. Larson, Finite element modeling of a linear membrane shell problem using tangential differential calculus, Comput. Methods Appl. Mech. Engrg. 270 (2014) 1–14.
[22] P. Hansbo, M. Larson, F. Larsson, Tangential differential calculus and the finite element modeling of a large deformation elastic membrane problem, Comput. Mech. 56 (1) (2015) 87–95.
[23] A. Klarbring, B. Torstenfelt, P. Hansbo, M.G. Larson, Optimal design of fibre reinforced membrane structures, Struct. Multidiscip. Optim. 56 (2017) 781–789.
[24] D. Schöllhammer, T.-P. Fries, Kirchhoff–Love shell theory based on tangential differential calculus, Comput. Mech. 64 (1) (2019) 113–131.
[25] T. van Opstal, E. van Brummelen, G. van Zwieten, A finite-element/boundary-element method for three-dimensional, large-displacement fluid–structure-interaction, Comput. Methods Appl. Mech. Engrg. 284 (2015) 637–663.
[26] O.C. Zienkiewicz, R.L. Taylor, The Finite Element Method, fifth ed., Butterworth-Heinemann, 2000.
[27] J.H. Argyris, I. Fried, D.W. Scharpf, The TUBA family of plate elements for the matrix displacement method, Aeronaut. J. 72 (692) (1968) 701–709.
[28] V. Dominguez, F.-J. Sayas, Algorithm 884: A simple matlab implementation of the argyris element, ACM Trans. Math. Softw. 35 (2) (2008) 16:1–16:11.
[29] K. Bell, A refined triangular plate bending finite element, Int. J. Numer. Methods Eng. 1 (1) (1969) 101–122.
[30] R.W. Clough, Finite element stiffness matricess for analysis of plate bending, in: Proc First Conf Matrix Methods Struct Mech, 1965, pp. 515–546.
[31] F. Cirak, M. Ortiz, P. Schröder, Subdivision surfaces: a new paradigm for thin-shell finite-element analysis, Int. J. Numer. Methods Eng. 47 (12) (2000) 2039–2072.
[32] F. Bogner, The generation of interelement-compatible stiffness and mass matrices by the use of interpolation formulas, in: Proc Conf Matrix Meth Struct Mech, Wright-Patterson AFB, 1965, pp. 397–443.
[33] E. Burman, P. Hansbo, M.G. Larson, Cut Bogner-Fox-Schmit elements for plates, Adv. Model Simul. Eng. Sci. 7 (1) (2020) 1–20.
[34] T. Hughes, J. Cottrell, Y. Bazilevs, Isogeometric analysis: CAD, finite elements, NURBS, exact geometry and mesh refinement, Comput. Methods Appl. Mech. Engrg. 194 (39) (2005) 4135–4195.
[35] J. Kiendl, K.-U. Bletzinger, J. Linhard, R. Wüchner, Isogeometric shell analysis with Kirchhoff-Love elements, Comput. Methods Appl. Mech. Engrg. 198 (49) (2009) 3902–3914.
[36] J.L. Batoz, C.L. Zheng, F. Hammadi, Formulation and evaluation of new triangular, quadrilateral, pentagonal and hexagonal discrete Kirchhoff plate/shell elements, Int. J. Numer. Methods Eng. 52 (5–6) (2001) 615–630.
[37] P.M.A. Areias, J.-H. Song, T. Belytschko, A finite-strain quadrilateral shell element based on discrete Kirchhoff-Love constraints, Int. J. Numer. Methods Eng. 64 (9) (2005) 1166–1206.
[38] W. Dornisch, R. Müller, S. Klinkel, An efficient and robust rotational formulation for isogeometric Reissner–Mindlin shell elements, Comput. Methods Appl. Mech. Engrg. 303 (2016) 1–34.
[39] R. Echter, B. Oesterle, M. Bischoff, A hierarchic family of isogeometric shell finite elements, Comput. Methods Appl. Mech. Engrg. 254 (2013) 170–180.
[40] K. Rafetseder, W. Zulehner, A new mixed approach to Kirchhoff–Love shells, Comput. Methods Appl. Mech. Engrg. 346 (2019) 440–455.
[41] M. Neunteufel, J. Schöberl, The Hellan-Herrmann-Johnson method for nonlinear shells, Comput. Struct. 225 (2019) 106109–106120.
[42] G. Engel, K. Garikipati, T.J. Hughes, M.G. Larson, L. Mazzei, R.L. Taylor, Continuous/discontinuous finite element approximations of fourth-order elliptic problems in structural and continuum mechanics with applications to thin beams and plates, and strain gradient elasticity, Comput. Methods Appl. Mech. Engrg. 191 (34) (2002) 3669–3750.

[43] P. Hansbo, M.G. Larson, Continuous/discontinuous finite element modelling of Kirchhoff plate structures in $\mathbb{R}^3$ using tangential differential calculus, Comput. Mech. 60 (4) (2017) 693–702.
[44] S. Bieber, B. Oesterle, E. Ramm, M. Bischoff, A variational method to avoid locking—independent of the discretization scheme, Internat. J. Numer. Methods Engrg. 114 (8) (2018) 801–827.
[45] T.X. Duong, F. Roohbakhshan, R.A. Sauer, A new rotation-free isogeometric thin shell formulation and a corresponding continuity constraint for patch boundaries, Comput. Methods Appl. Mech. Engrg. 316 (2017) 43–83.
[46] A.J. Herrema, E.L. Johnson, D. Proserpio, M.C. Wu, J. Kiendl, M.-C. Hsu, Penalty coupling of non-matching isogeometric Kirchhoff–Love shell patches with application to composite wind turbine blades, Comput. Methods Appl. Mech. Engrg. 346 (2019) 810–840.
[47] L. Leonetti, F.S. Liguori, D. Magisano, J. Kiendl, A. Reali, G. Garcea, A robust penalty coupling of non-matching isogeometric Kirchhoff–Love shell patches in large deformations, Comput. Methods Appl. Mech. Engrg. 371 (2020) 113289.
[48] K. Paul, C. Zimmermann, T.X. Duong, R.A. Sauer, Isogeometric continuity constraints for multi-patch shells governed by fourth-order deformation and phase field models, Comput. Methods Appl. Mech. Engrg. 370 (2020) 113219.
[49] T. Pasch, L. Leidinger, A. Apostolatos, R. Wüchner, K.-U. Bletzinger, F. Duddeck, A priori penalty factor determination for (trimmed) NURBS-based shells with Dirichlet and coupling constraints in isogeometric analysis, Comput. Methods Appl. Mech. Engrg. 377 (2021) 113688.
[50] L. Coradello, J. Kiendl, A. Buffa, Coupling of non-conforming trimmed isogeometric Kirchhoff–Love shells via a projected super-penalty approach, Comput. Methods Appl. Mech. Engrg. 387 (2021) 114187.
[51] H. Zhao, X. Liu, A.H. Fletcher, R. Xiang, J.T. Hwang, D. Kamensky, An open-source framework for coupling non-matching isogeometric shells with application to aerospace structures, Comput. Math. Appl. 111 (2022) 109–123.
[52] A. Farahat, H.M. Verhelst, J. Kiendl, M. Kapl, Isogeometric analysis for multi-patch structured Kirchhoff–Love shells, Comput. Methods Appl. Mech. Engrg. 411 (2023) 116060.
[53] G. Dziuk, C. Elliott, Finite element methods for surface PDEs, Acta. Numer. 22 (2013) 289–396.
[54] S. Rosenberg, the Laplacian on a Riemannian Manifold: An Introduction To Analysis on Manifolds, in: London Mathematical Societyn, No. 31, Cambridge University Press, 1997.
[55] J.E. Marsden, T.J. Hughes, Mathematical Foundations of Elasticity, Prentice-Hall, Englewood Cliffs, 1983.
[56] P.G. Ciarlet, Mathematical Elasticity: Three-Dimensional Elasticity, I ed., North-Holland, Amsterdam, 1988.
[57] R. Kupferman, A. Shachar, A geometric perspective on the Piola identity in Riemannian settings, J. Geom. Mech. 11 (1) (2019) 59.
[58] T.J.R. Hughes, J.A. Cottrell, Y. Bazilevs, Isogeometric analysis: CAD, finite elements, NURBS, exact geometry and mesh refinement, Comput. Methods Appl. Mech. Engrg. 194 (39) (2005) 4135–4195.
[59] L. Piegl, W. Tiller, The NURBS Book, in: Monographs in Visual Communication, Springer-Verlag, Berlin Heidelberg, 1995.
[60] P.G. Ciarlet, An Introduction To Differential Geometry with Applications To Elasticity, Vol. 78, Springer, 2006.
[61] G. Radenković, A. Borković, B. Marussig, Nonlinear static isogeometric analysis of arbitrarily curved Kirchhoff-Love shells, Int. J. Mech. Sci. 192 (2021) 106143.
[62] M.H. Gfrerer, M. Schanz, High order exact geometry finite elements for seven-parameter shells with parametric and implicit reference surfaces, Comput. Mech. (2018) 1–13.